Am J Transl Res 2020;12(6):2379-2395
www.ajtr.org /ISSN:1943-8141/AJTR0107576

Original Article

Two-layer regulation of *TRAF6* mediated by both TLR4/NF-kB signaling and miR-589-5p increases proinflammatory cytokines in the pathology of severe acute pancreatitis

Zhi Chen[1], Wei-Hua Dong[1], Qi Wu[1], Jun Wang[2]

Departments of [1]Critical Care Medicine, [2]General Surgery, Jiangxi Provincial People's Hospital Affiliated to Nanchang University, Nanchang, Jiangxi, China

Received January 8, 2020; Accepted April 24, 2020; Epub June 15, 2020; Published June 30, 2020

Abstract: Inflammation is a leading cause of severe acute pancreatitis (SAP). MicroRNAs (miRNAs) are emerging as important regulators involved in the pathogenesis of many diseases including pancreatitis. To identify miRNAs that contribute to the pathology of SAP, we carried out a miRNA-specific microarray analysis using the biopsies donated by SAP patients. We totally obtained 50 differentially expressed miRNAs, including 20 upregulated and 30 downregulated miRNAs, respectively. We focused our current study on revealing the downstream target and the upstream regulatory mechanism of miR-589-5p, the most downregulated miRNA in our candidate lists. Our prediction results indicated that miR-589-5p might target *TRAF6* (tumor necrosis factor receptor-associated factor 6), a critical member of the TLR4/NF-kB (Toll-like receptor 4/nuclear transcription factor-kB) pathway. Using different strategies such as *in vitro* overexpression or downregulation of miR-589-5p and treatment with lipopolysaccharide (LPS), we found that the expression of *TRAF6* was regulated by two-layer mechanisms. On the one hand, *TRAF6* was transcriptionally controlled by a DNA methylation mediated downregulation of miR-589-5p. On the other hand, the activation of TLR4/NF-kB signaling also could increase the protein level of TRAF6. The increased TRAF6 aggravated the downstream signaling and caused the translocation of NF-kB subunits from the cytoplasm to the nucleus, where NF-kB transcription factors induced the expression of proinflammatory cytokine genes. The maturation and production of proinflammatory cytokines induced inflammatory response and caused the occurrence of SAP.

Keywords: Serve acute pancreatitis, miRNA, miR-589-5p, TRAF6, NF-kB

Introduction

Severe acute pancreatitis (SAP) is a serious disorder with high morbidity and mortality [1, 2]. With the rapid elevation of proinflammatory cytokines in the early stage of SAP, inflammatory response progresses to the pancreatic necrosis, eventually causing a systemic inflammatory response syndrome (SIRS) and multisystem organ failure (MOF) [1, 2]. Apparently, inflammation is a leading cause of SAP [1, 2]. In the early stage of SAP, injured and dead acinar cells in the pancreas release damage-associated molecular patterns (DAMPs), which act as endogenous danger stimuli to activate and exacerbate the inflammatory response by affecting macrophages [3, 4]. The activated immune cells augment cytokine signaling pathways and lead to the increase of proinflammatory cytokines such as interleukin-1 beta (IL-1β), IL-6, IL-8 and tumor necrosis factor-alpha (TNF-α) [3, 4].

The regulation of proinflammatory cytokines has been well characterized in different inflammatory diseases [5-8]. Multiple signaling pathways, such as the Toll-like receptor 4/nuclear transcription factor-kB (TLR4/NF-kB) axis signaling, the Janus kinase/signal transducers and activator of transcription (JAK/STAT) axis signaling, and the transforming growth factor-β/Mothers against decapentaplegic homolog (TGF-β/SMAD) axis signaling, can participate in the regulation of proinflammatory cytokine genes [5-8]. In a number of inflammatory diseases including pancreatitis, the lipopolysaccha-

ride (LPS)-stimulated TLR4 undergoes oligomerization and recruits its downstream adaptors, including TRIF (TIR domain-containing adaptor inducing IFN-β), TIRAP (TIR domain-containing adaptor protein), TRAM (TRIF-related adaptor molecule), and MyD88 (myeloid differentiation primary response gene 88) [10, 11]. MyD88 further activates IRAK4 (IL-1 receptor-associated kinase-4), which is required for the activation and degradation of IRAK1 [10, 11]. The activated IRAK1 phosphorylates TRAF6 (tumor necrosis factor receptor-associated factor 6), enabling the formation of a complex with UEV1A (ubiquitin-conjugating enzyme E2 variant 1 isoform A) and UBC13 (ubiquitin-conjugating enzyme 13 [10, 11]. This complex initiates a kinase cascade that includes TAK1 (transforming growth factor-β-activated kinase 1) and IKKs (IκB kinase). IKKs phosphorylate IκB (inhibitor of κ light chain gene enhancer in B cells) proteins and cause its degradation, thereby abolishing the inhibitory effect of IκB on NF-κB subunits [10, 11]. The released NF-κB subunits translocate from the cytoplasm to the nucleus, where they induce the expression of proinflammatory cytokine genes such as *IL-1B*, *IL-6*, *IL-8* and *TNFA* [10, 11]. A few studies have demonstrated that the activation of NF-κB increases the severity of pancreatitis [12, 13]. TGF-β signaling is essential for the maintenance of immune homeostasis and the suppression of autoimmunity [14]. In a mouse model, Hahm and colleagues found that the downregulation of TGF-β signaling can result in autoimmune pancreatitis [15]. MAPK cascades play important roles in the early events of acute pancreatitis (AP) because they are required for the phosphorylation of several transcription factors [e.g., NF-kB and c-JUN] that regulate the expression of inflammatory cytokines [16, 17]. MAPK inhibitors exhibit promising effects on the treatment of AP by repressing the expression of proinflammatory cytokines [18]. The JAK/STAT signaling is also involved in the pathology of pancreatitis by affecting the proliferation of pancreatic stellate cells [19]. Komar and colleagues found the JAK inhibitor ruxolitinib can reduce the severity of pancreatitis [19].

MicroRNAs (miRNAs) are a class of noncoding RNAs with 18-25 nucleotides [20]. Currently, more than 2000 miRNAs have been discovered in the human genome [21]. Mechanistically, miRNAs repress gene expression by guiding Argonaute (AGO) proteins to the 3'-untranslated region (3'-UTR) of their target mRNAs, where AGOs form a complex known as miRNA-induced silencing complex (miRISC). The miRISC represses the translation of its targeted mRNAs and causes their degradation [22, 23]. Emerging evidence suggests that miRNAs play critical roles in different biological processes (e.g., cell differentiation, DNA damage and repair, cell cycle progression and apoptosis) and are widely involved in the pathogenesis of many diseases including pancreatitis [24-26]. Liu and colleagues found that serum-circulating miR-7, miR-10, and miR-92b were significantly decreased in AP patients and suggested that these miRNAs might be used as the diagnostic and prognostic biomarkers for AP patients [27]. Kusnierz-Cabala and colleagues demonstrated that miR-126-5p and miR-551b-5p were significantly increased in mild and SAP patients and their statistical results showed that these two miRNAs could predict the severity of AP [28]. In the hypertriglyceridemia-induced AP patients, four miRNAs, including miR-24-3p, miR-222-3p, miR-361-5p and miR-1246, were remarkably increased, while miR-181a-5p was dramatically downregulated [29]. Although miRNAs are widely involved in the pathogenesis of pancreatitis, little is known about their target genes and their contributions to the signaling pathways in which their target genes are involved. Another issue is that the molecular mechanisms regarding the aberrant expression of miRNAs are unclear.

To evaluate whether TLR4/NF-kB signaling is activated in the SAP patients, we found the elevated levels of several proinflammatory cytokines, including IL-1β, IL-6, IL-8, IL-15, IFN-γ and TNF-α, whose encoding genes are all the NF-kB target genes. Several critical members of TLR4/NF-kB signaling pathways, including TLR4, TRAF6, IKK1 and IkB, were also detected to verify the activation of this signaling pathway. To identify the differentially expressed miRNAs in the SAP patients, we conducted a microarray analysis and found that miR-589-5p was significantly downregulated in the SAP patients, and it was predicted to target *TRAF6*. We then performed *in vitro* analyses to reveal that *TRAF6* was coregulated by both miR-589-5p and TLR4 signaling. The amplified TRAF6 activated the NF-kB transcription factor, there-

by upregulating the expression of proinflammatory cytokine genes. Our results provide a detailed miRNA profile in the SAP patients and may benefit our understanding of how miRNAs are regulated and how they contribute to the pathogenesis of SAP.

Materials and methods

Blood and pancreatic sample collection

Blood samples were venously drawn from healthy volunteers (n=48) and SAP patients (n=48), respectively, and stored in the EDTA-coated blood collection tubes (Pulmolab, Northridge, CA, USA, #367861). The concentrations of cytokines in blood samples were measured using their corresponding ELISA kits, including IL-1β (Thermo Fisher Scientific, Waltham, MA, USA, #KAC1211), IL-4 (#KAC1281), IL-6 (#KHC0061), IL-8 (#KHC0081), IL-10 (#KAC1321), IL-13 (#BMS231INST), IL-15 (#BMS2106), IFN-γ (#EHIFNG), and TNF-α (#KHC3011). The pancreatic tissues were collected from 24 pancreatic cancer patients (under stage 0, control) and 24 SAP patients according to the endoscopic ultrasound-guided fine-needle aspiration (EUS-FNA) method [30]. The information of these patients was included in Tables S1 and S2. All participants were informed of the purpose of this study and signed a consent form reviewed and approved by the ethical board of Jiangxi Provincial People's Hospital in China.

Protein extraction and immunoblots

The cultured cells and pancreatic biopsies from pancreatic cancer patients and SAP patients were subjected to extract total protein with 1 × RIPA buffer (Sigma-Aldrich, Shanghai, China, #R0278). After quantification of protein concentrations, equal amounts of proteins were loaded onto 10% SDS-PAGE gels for separation, followed by transferring to PVDF membranes (GE Healthcare, Chicago, IL, USA, #10600023). The membranes were then probed with primary antibodies including anti-TLR4 (Abcam, #ab22048, Shanghai, China), anti-TRAF6 (Abcam, #ab137452), anti-IKK1 (Abcam, #ab227852), anti-IkB (Sigma-Aldrich, Shanghai, China, #HPA029207), anti-pIkB (Abcam, #ab133462), anti-RELA (Santa Cruz Biotechnology, Dallas, TX, USA, #sc-8008), anti-RELB (Thermo Fisher Scientific, #PA5-27679), anti-c-REL (Abcam, #ab227519), anti-NFKB1 (Abcam, #ab195854), anti-NFKB2 (Abcam, #ab131539), anti-GAPDH (Abcam, #ab8254), anti-β-Actin (Abcam, #ab179467), and anti-LSD1 (Abcam, #ab62582). After probing with secondary antibodies, protein signals were detected with an ECL kit (Thermo Fisher Scientific, #32106).

Microarray analysis and miRNA detection

Three-paired pancreatic biopsies from controls and SAP patients were subjected to miRNA isolation using a miRNeasy Mini Kit (QIAGEN, Shanghai, China, #217004) following the manufacturer's instructions. The resulting miRNAs were used for microarray analyses and to examine the differentially expressed miRNAs. In brief, 500 ng miRNA of each sample was applied to microarray using a GeneChip™ miRNA 4.0 Chip (Thermo Fisher Scientific, #902445) following a protocol provided by the manufacturer. Chip slides were scanned in an Agilent SureScan Dx Microarray Scanner (Agilent, Beijing, China, #G5761AA). For miRNA quantification, the expression levels of miR-let-7e, miR-20b-5p, miR-127-3p, miR-194-5p, miR-411-3p, and miR-589-5p were examined by qRT-PCR using different TaqMan microRNA assays: #478579 (miR-let-7e), #477804 (miR-20b-5p), #477889 (miR-127-3p), #477956 (miR-194-5p), #479526 (miR-411-3p), and #479073 (miR-589-5p), respectively.

Primary pancreatic acinar cell isolation and culture

The isolation of primary pancreatic acinar cells (PPAC) was performed following a previous method with modification [31]. Briefly, three-paired pancreatic biopsies were collected from pancreatic cancer patients (stage 0) and SAP patients using the EUS-FNA method. The biopsies were rinsed twice in Hank's Balanced Salt Solution (HBSS) (Thermo Fisher Scientific, #14025076), followed by slicing the pancreases into small pieces (~1 mm^3). The resulting slices were treated with collagenase IA solution containing 10 mM HEPES-KOH (pH 8.0), 200 U/mL collagenase IA (Sigma-Aldrich, #C9891), and 0.25 mg/mL trypsin inhibitor (Sigma-Aldrich, #T9253) to enzymatically digest and mechanically dissociate the pancreases. After centrifugation, the pellets were resuspended in Waymouth's medium (Thermo Fisher Scientific,

#11220035) supplemented with 2.5% fetal bovine serum (FBS) (Thermo Fisher Scientific, #26140079), 1% penicillin-streptomycin (PS) (Thermo Fisher Scientific, #10378016), 0.25 mg/mL trypsin inhibitor, and 25 ng/mL recombinant human epidermal growth factor (EGF) (Thermo Fisher Scientific, #RP-8661). The cell suspension was filtrated with a 100 μm filter (Sigma-Aldrich, #CLS431752) to retain the non-digested fragments, followed by culturing in a humidified incubator containing 5% CO_2 at 37°C.

Cell culture and cell transfection

A human pancreatic epithelial cell line MIA PaCa-2 (#CRL-1420) and a human macrophage cell line THP-1 (#TIB-202) were purchased from ATCC (American Type Culture Collection) (Manassas, VA, USA). Both of them were grown in DMEM medium (Sigma-Aldrich, #D6046) containing 10% FBS and 1% PS with the medium change every three days. Cells under 60%-80% confluence were used for transfections with miR-589-5p-mimic and anti-miR-589-5p (RiboBio, Guangzhou, China) following the manufacturer's protocol. After culturing for another 48 h, the transfected cells were harvested and applied to the required experiments.

Total RNA isolation and qRT-PCR analysis

The cultured cells and pancreatic tissues were subjected to total RNA isolation with a TRIzol reagent (Thermo Fisher Scientific, #15596026) following a method provided by the manufacturer. After determining total RNA concentrations with a Nanodrop spectrophotometer (Thermo Fisher Scientific, #ND-2000), 1.0 mg RNA was used to synthesize cDNA with a reverse transcription kit (Thermo Fisher Scientific, #4368814). The cDNAs were diluted 20-fold, followed by qRT-PCR analyses to detect gene expression with primers included in Table S3.

*Treatments with 5-aza-2'-deoxycytidine (AZA) and trichostatin A (*TSA*)*

The PPAC cells from a pancreatic cancer patient (PPAC-H1) and an SAP patient (PPAC-P1) were treated with different concentrations of AZA (0, 2.5 and 25 mM) and TSA (0, 2.5 and 25 mM), respectively, for 6 h. Cells were then rinsed twice with PBS buffer and then were subjected to the required experiments.

Quantitative methylation-specific PCR (qMSP) analysis

The qMSP analysis was carried out according to a previous method [26]. In brief, the AZA-treated cells were used for genomic DNA isolation with a kit (Thermo Fisher Scientific, #K182001) following the manufacturer's method. For each sample, 1 μg DNA was treated with sodium bisulfite using an EZ DNA Methylation-GOLD kit (Zymo Research, Tustin, CA, USA, #D5006) according to the manufacturer's method. The obtained genomic DNA was diluted 10-fold and then used for qMSP analysis with a TaqMan Universal Master Mix II non-UNG Kit (Thermo Fisher Scientific, #4440038). Primers used for qMSP analysis were included in Table S4.

Statistical analysis

All experiments in the current study were independently performed in triplicate. The data were statistically analyzed using a two-sided Student's t test. The significant difference was defined following a standard of $P < 0.05$ (*), $P < 0.01$ (**) and $P < 0.001$ (***).

Results

The proinflammatory cytokine levels were increased in the SAP patients

Previous publications have shown that the serum concentrations of some proinflammatory cytokines (e.g., TNF-α, IL-1β, IL-6 and IL-8) are elevated in SAP patients [1-7]. To solid this conclusion, we collected blood samples from healthy volunteers (control, n=48) and SAP patients (n=48) and determined the circulating concentrations of six proinflammatory cytokines (IL-1β, IL-6, IL-8, IL-15, INF-γ and TNF-α) and three anti-inflammatory cytokines (IL-4, IL-10 and IL-13) using ELISA assays. Our results indicated that the average values of all six detected proinflammatory cytokines were significantly increased in the SAP samples compared to healthy controls (**Figure 1A-F**). However, the average concentrations of three anti-inflammatory cytokines were not dramatically changed (**Figure 1G-I**). These results supported the previous conclusion that circulating proinflammatory cytokines were elevated in the SAP patients.

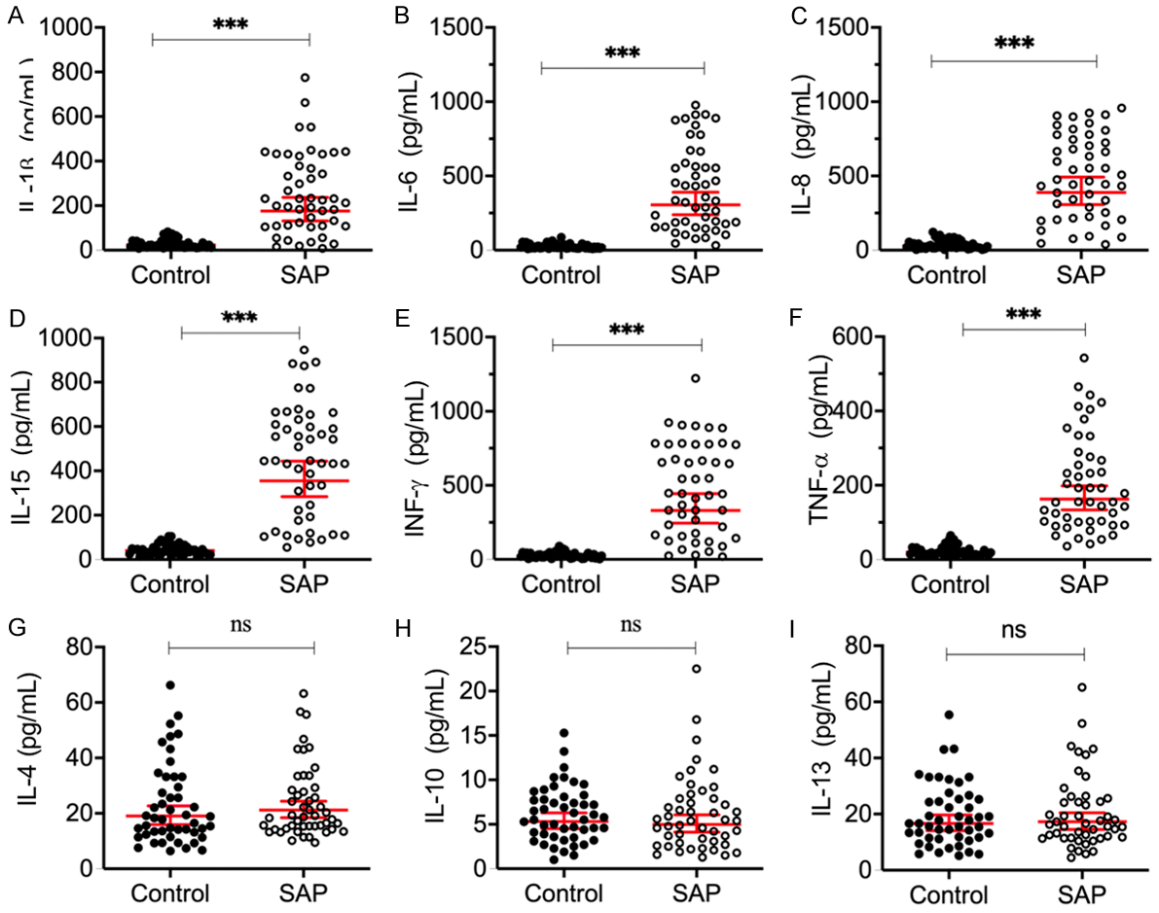

Figure 1. The concentrations of proinflammatory cytokines were increased in SAP patients. Circulating levels of IL-1β (A), IL-6 (B), IL-8 (C), IL-15 (D), INF-γ (E), TNF-α (F), IL-4 (G), IL-10 (H), and IL-13 (I) were measured in blood samples collected from healthy controls (n=48) and SAP patients (n=48) using ELISA assays. ***$P < 0.001$. ns represented no significant difference.

The TLR4/NF-kB signaling pathway was activated in the SAP patients

The coding genes of those elevated proinflammatory cytokines are all the downstream targets of NF-kB [3-7], which implied that NF-kB and its upstream signaling might be activated in the SAP patients. To verify this hypothesis, we examined several members of the TLR4/NF-kB signaling pathway, including TLR4, TRAF6, IKK1 and IkB, in three-paired pancreatic tissues from controls and SAP patients. Our results showed that the protein levels of TLR4, TRAF6 and IKK1 were significantly increased (~2.5-5.0-fold) in the SAP patients compared to controls (**Figures 2A** and S1A). IkB was remarkably decreased (~2.5-fold), whereas its phosphorylation protein (pIkB) was significantly increased (~2.2-fold) in the SAP patients (**Figures 2A** and S1A). Because IkB functions as an inhibitor of NF-kB, we next sought to examine the protein levels of NF-kB subunits in the three-paired pancreatic tissues. Intriguingly, we did not observe visible changes in the levels of NF-kB subunits, including RELA (p65), RELB, c-REL, NFKB1 (p50) and NFKB2 (p52) in the total extracts (**Figures 2B** and S1B). It has been well studied that NF-kB subunits translocate from the cytoplasm to the nucleus once they are activated [3-7]. Thus, we separated the nuclear and cytoplasmic fractions and then evaluated the distribution of NF-kB subunits in these two fractions. As expected, our results showed that all the five subunits were decreased (~1.8-2.1-fold) in the cytoplasm but significantly increased (~2.1-3.0-fold) in the nucleus from pancreatic tissues (**Figures 2C**, **2D**, S1C and S1D). These results suggested that the TLR4/NF-kB signaling pathway was activated in the SAP patients.

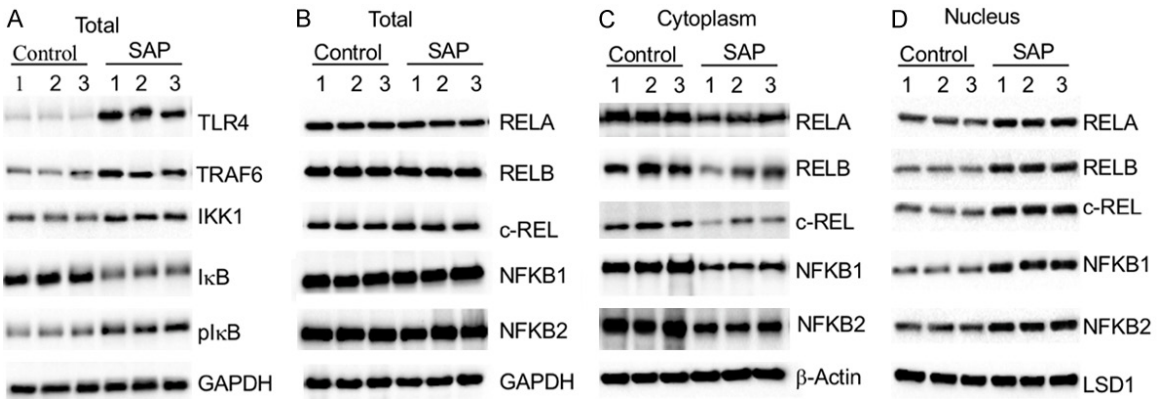

Figure 2. The TLR4/NF-kB signaling was activated in SAP patients. (A) The protein levels of several members of the TLR4/NF-kB signaling pathway were elevated *in vivo*. Total cell extracts of three-paired pancreatic tissues from controls (pancreatic cancer patients, stage 0) and SAP patients were subjected to immunoblot analyses to examine the protein levels of TLR4, TRAF6, IKK1, IkB and pIkB. GAPDH was used as a loading control. (B) The protein levels of NF-kB subunits in total cell extracts were not changed between controls and SAP patients. The same cell extracts used in (A) were applied to immunoblot analyses to examine the protein levels of RELA, RELB, c-REL, NFKB1 and NFKB2. GAPDH was used as a loading control. (C) The protein levels of NF-kB subunits in cytoplasmic fractions were significantly decreased in SAP tissues compared to controls. β-Actin was used as a loading control. (D) The protein levels of NF-kB subunits in nuclear fractions were significantly increased in SAP tissues compared to controls. LSD1 (Lysine-specific histone demethylase 1) was used as a loading control.

Identification of differentially expressed miRNAs in the pancreatic tissues from SAP patients

In recent years, a few miRNAs have been found to be differentially expressed in chronic pancreatitis patients and animal models [26]. To determine if miRNAs are also involved in the pathogenesis of SAP, especially in the regulation of TLR4/NF-kB signaling, we carried out a microarray analysis using RNA from three-paired pancreatic tissues of controls and SAP patients (same as the tissues used in **Figure 2**). Totally, we identified 50 differentially expressed miRNAs in the SAP patients compared to controls (Table S5). Of them, 20 miRNAs were upregulated, while the other 30 were downregulated (Table S5). As shown in **Figure 3A**, we presented 10 miRNAs that were consistently upregulated or downregulated in SAP-sourced samples. We then randomly selected three upregulated miRNAs (miR-let-7e, miR-127-3p and miR-411-3p) and three downregulated miRNAs (miR-20b-5p, miR-194-5p and miR-589-5p) and examined their expression levels in the pancreatic tissues from controls (n=24) and SAP patients (n=24). Similar to the microarray results, our results indicated that the expression levels of miR-20b-5p, miR-194-5p and miR-589-5p were significantly upregulated while the expression levels of miR-20b-5p, miR-194-5p and miR-589-5p were markedly decreased in the 24 SAP patients compared to the controls (**Figure 3B-G**). To evaluate whether these differentially expressed miRNAs participated in the regulation of TLR4/NF-kB signaling, we predicted their potential targets in a database (http://www.mirdb.org/miRDB). We found that only miR-589-5p was predicted to target *TRAF6* (Table S6).

TRAF6 was a direct target of miR-589-5p

To verify whether *TRAF6* was a direct target of miR-589-5p, we next sought to identify the binding site of miR-589-5p in the 3'-UTR of *TRAF6*. As shown in **Figure 4A**, we found four sites that were potentially bound by the seed sequence (CAAGAGU) of miR-589-5p. These sites located in the following nucleotide regions: 59-65, 474-480, 539-545 and 1273-1279. To determine which site was necessary for the binding of miR-589-5p, we created different vectors containing *TRAF6* coding sequences (CDS) and either its wild type (WT) or mutated 3'-UTRs (**Figure 4B**): pcDNA3-TRAF6-3'-UTR^{WT}, pcDNA3-TRAF6-3'-UTR$^{Mut\,(59\text{-}65)}$, pcDNA3-TRAF6-3'-UTR$^{Mut\,(474\text{-}480)}$, pcDNA3-TRAF6-3'-UTR$^{Mut\,(539\text{-}545)}$, and pcDNA3-TRAF6-3'-UTR$^{Mut\,(1273\text{-}1279)}$. We then co-transfected the individual WT or mutated vector together with miR-589-5p-mimic into the human pancreatic epithelial cell line MIA

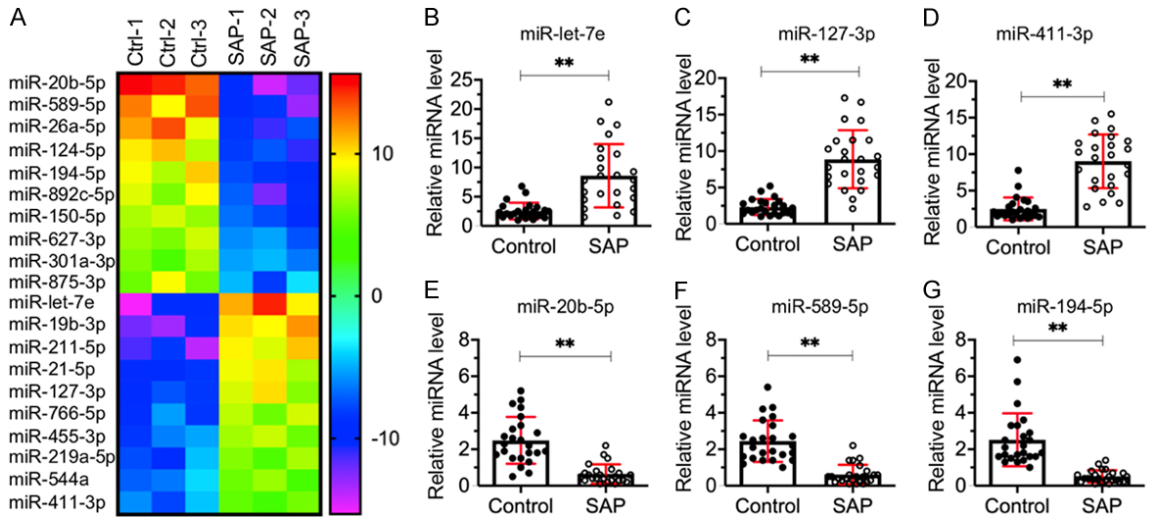

Figure 3. Identification and verification of differentially expressed miRNAs in SAP patients. (A) Heatmaps of the top 10 upregulated and downregulated miRNAs. MiRNAs from three-paired pancreatic tissues from controls (pancreatic cancer patients, stage 0) and SAP patients were subjected to microarray analysis. The top 10 upregulated or downregulated miRNAs in SAP tissues were shown. (B-G) Verification of miRNA expression levels. Twenty-four paired pancreatic tissues from controls and SAP patients were subjected to miRNA isolation and qRT-PCR analyses to measure the expression levels of three upregulated miRNAs including miR-let-7e (B), miR-127-3p (C), and miR-411-3p (D), and three downregulated miRNAs including miR-20b-5p (E), miR-589-5p (F), and miR-194-5p (G). $^{**}P < 0.01$.

PaCa-2. After verifying the successful transfection of miR-589-5p (**Figure 4C**), we evaluated the effects of miR-589-5p overexpression on *TRAF6* expression in cells harboring the WT and mutated 3'-UTRs. As shown in **Figure 4D**, miR-589-5p overexpression significantly decreased *TRAF6* mRNA levels in cells harboring WT 3'-UTR. In contrast, we also fund that miR-589-5p overexpression could decrease the expression of *TRAF6* in cells harboring mutated 3'-UTR (**Figure 4D**). However, the expression levels of *TRAF6* in cells harboring mutated 3'-UTR were much higher than that of in cells harboring WT 3'-UTR (**Figure 4D**). Comparing the expression levels of *TRAF6* in cells harboring four different mutants, we did not observe a significant difference (**Figure 4D**). These results suggested that *TRAF6* was a direct target of miR-589-5p and that all of these four sites containing GTTCTCA in the 3'-UTR of *TRAF6* were required for miR-589-5p binding.

In vitro repression of miR-589-5p could activate the TRAF6 downstream signaling in the condition without LPS treatment

Since *TRAF6* was a direct target of miR-589-5p, we speculated that overexpression or inhibition of miR-589-5p should affect the downstream signaling of TRAF6. To verify this hypothesis, we transfected the THP-1 and MIA PaCa-2 cells with miR-NC (control), miR-589-5p-mimic or anti-miR-585-5p and evaluated the effects of overexpression or inhibition of miR-589-5p on TLR4/NF-kB signaling. After examining the successful transfection of miR-NC, miR-589-5p-mimic and anti-miR-585-5p (Figure S2), we found that overexpression of miR-589-5p caused the downregulation of *TRAF6* mRNA level, while the repression of miR-589-5p resulted in the overexpression of *TRAF6* mRNA level in both THP-1 and MIA PaCa-2 backgrounds (Figure S2). Thus, we next measured the protein levels of TLR4, TRAF6, IKK1, IkB and pIkB in the THP-1 cell background as a representation. Our results indicated that the protein levels of TRAF6, IKK1 and pIkB were remarkably decreased (~2.1-4.8-fold), while IkB was significantly increased (~2.0-fold) in cells overexpressing miR-589-5p compared to the control (**Figures 5A** and S3A). In contrast, we found that inhibition of miR-589-5p increased TRAF6, IKK1 and pIkB levels (~1.7-1.9-fold) but decreased IkB levels (~1.4-fold) (**Figures 5A** and S3A). However, neither miR-589-5p overexpression nor inhibition could change TLR4 protein levels (**Figures 5A** and S3A). Next, we measured the total, cytoplasmic and nuclear protein levels of NF-kB subunits under the condi-

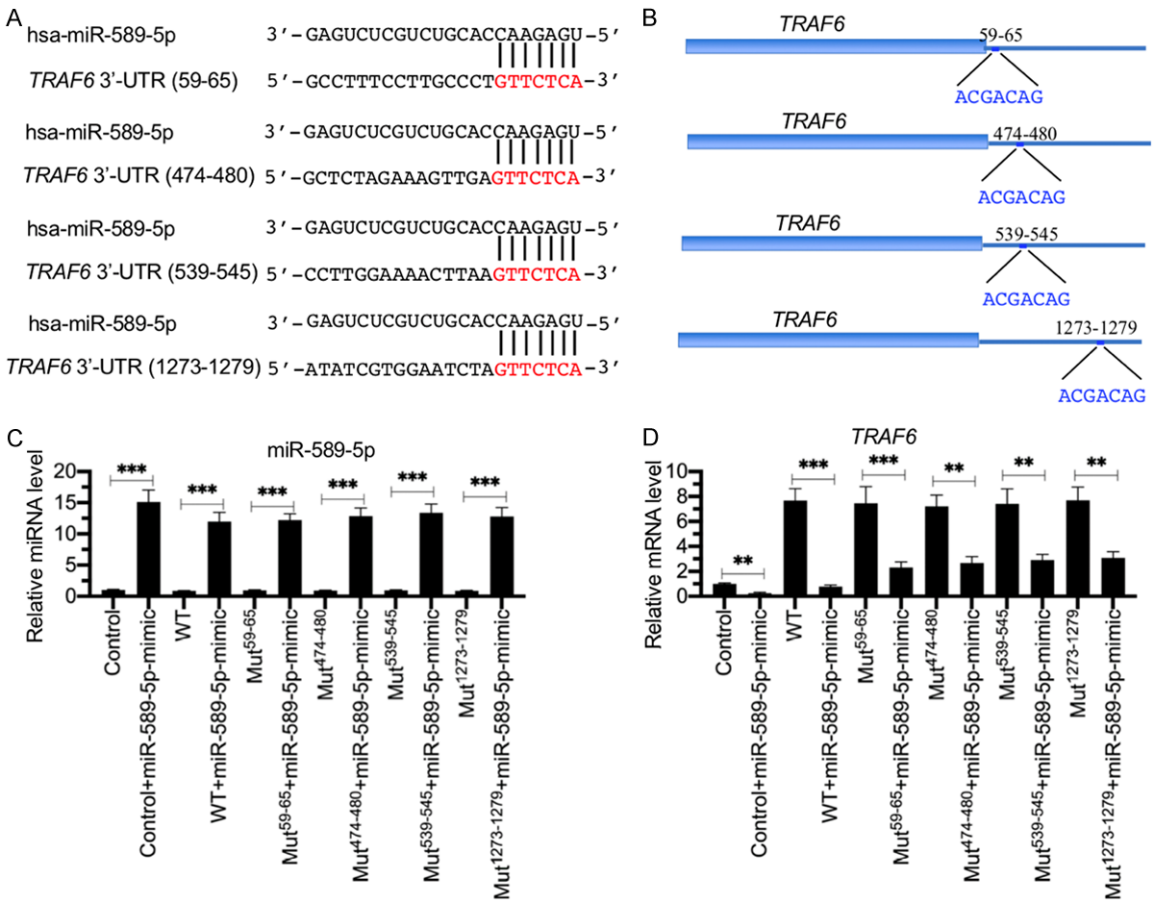

Figure 4. *TRAF6* was a direct target of miR-589-5p. (A) The 3'-UTR of *TRAF6* contained four miR-589-5p binding sites. The seed sequence of miR-589-5p (CAAGAGU) can bind to four positions corresponding to nucleotide regions 59-65, 474-480, 539-545 and 1273-1279 in the 3'-UTR of *TRAF6*. The sequence of miR-589-5p and its binding sites were shown. (B) Schematic representations of mutations in the 3'-UTR of *TRAF6*. The mutated nucleotides were shown in blue. (C) Relative miR-589-5p levels. The TRAF6 CDS sequence and its WT and mutated 3'-UTRs were cloned into the pcDNA3 vector. Different combinations of the following plasmids and mimics were transfected into MIA PaCa-2 cells: pcDNA3+miR-NC (Control); pcDNA3+miR-589-5p-mimic (Control+miR-589-5p-mimic); pcDNA3-TRAF6-3'-UTR^{WT}; pcDNA3-TRAF6-3'-UTR^{WT}+miR-589-5p-mimic; pcDNA3-TRAF6-3'-UTR$^{Mut\ (59\text{-}65)}$; pcDNA3-TRAF6-3'-UTR$^{Mut\ (59\text{-}65)}$+miR-589-5p-mimic; pcDNA3-TRAF6-3'-UTR$^{Mut\ (474\text{-}480)}$; pcDNA3-TRAF6-3'-UTR$^{Mut\ (474\text{-}480)}$+miR-589-5p-mimic; pcDNA3-TRAF6-3'-UTR$^{Mut\ (539\text{-}545)}$; pcDNA3-TRAF6-3'-UTR$^{Mut\ (539\text{-}545)}$+miR-589-5p-mimic; pcDNA3-TRAF6-3'-UTR$^{Mut\ (1273\text{-}1279)}$; and pcDNA3-TRAF6-3'-UTR$^{Mut\ (1273\text{-}1279)}$+miR-589-5p-mimic. After incubation for 48 h, cells were collected to measure miR-589-5p levels. ***P < 0.001. (D) Relative *TRAF6* levels. Cells used in (C) were applied to measure *TRAF6* expression levels using qRT-PCR. **P < 0.01 and ***P < 0.001.

tions of miR-589-5p overexpression and inhibition. As shown in **Figures 5B** and S3B, we did not observe an apparent change in NF-kB subunits in the total cell extracts. However, we found a significant increase (~2.2-2.7-fold) in all NF-kB subunits in the cytoplasmic fraction when miR-589-5p was overexpressed (**Figures 5C** and S3C). In contrast, miR-589-5p inhibition caused a slight decrease (~1.3-1.5-fold) in all NF-kB subunits in the cytoplasmic fraction (**Figures 5C** and S3C). All NF-kB subunits in the nuclear fractions were dramatically decreased (~2.3-5.1-fold) after miR-589-5p overexpression, while they were upregulated (~1.6-1.8-fold) when miR-589-5p was inhibited (**Figures 5D** and S3D). Since miR-589-5p overexpression and inhibition can affect the cytoplasm-nucleus translocation of NF-kB subunits, we next sought to determine if they can change the expression of downstream targets of NF-kB. The qRT-PCR results showed that all seven NF-kB targets including *IL-1B*, *IL-6*, *IL-8*, *TNFA*, *IFNG* (interferon-gamma), *CCL3* (C-C motif chemokine ligand 3) and *LTA* (lymphotoxin alpha) were downregulated in cells expressing miR-589-5p-mimic but upregulated in cells harbor-

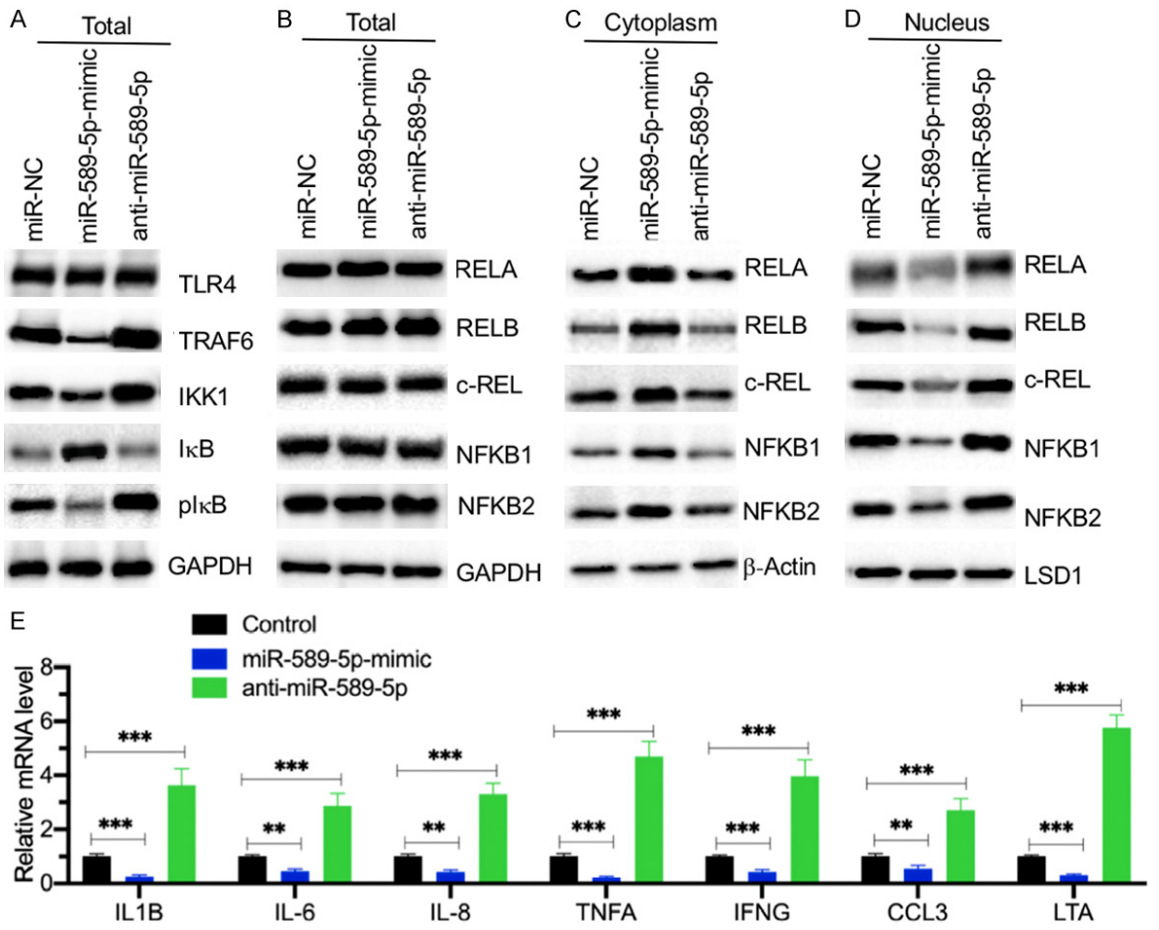

Figure 5. Overexpression or downregulation of miR-589-5p affected the TLR4/NF-kB signaling. (A) Changes in miR-589-5p levels affected the protein levels of several members of the TLR4/NF-kB signaling pathway. Total cell extracts from MIA PaCa-2 cells transfected with miR-NC, miR-589-5p-mimic and anti-miR-589-5p were subjected to immunoblot analyses to examine the protein levels of TLR4, TRAF6, IKK1, IkB and pIkB. GAPDH was used as a loading control. (B) Changes in miR-589-5p levels did not affect NF-kB subunit protein levels in total extracts. The same cell extracts used in (A) were applied to immunoblot analyses to examine the protein levels of RELA, RELB, c-REL, NFKB1 and NFKB2. GAPDH was used as a loading control. (C) The protein levels of NF-kB subunits in the cytoplasmic fractions. The cytoplasmic fractions from MIA PaCa-2 cells transfected with miR-NC, miR-589-5p-mimic and anti-miR-589-5p were subjected to immunoblot analyses to examine NF-kB subunit protein levels. β-Actin was used as a loading control. (D) The protein levels of NF-kB subunits in nuclear fractions. The nuclear fractions from MIA PaCa-2 cells transfected with miR-NC, miR-589-5p-mimic and anti-miR-589-5p were subjected to immunoblot analyses to examine NF-kB subunit protein levels. LSD1 was used as a loading control. (E) Changes in miR-589-5p levels affected the expression of NF-kB targets. Cells used in (A) were used for RNA isolation and qRT-PCR analyses to measure the expression of NF-kB targets, including *IL-1B*, *IL-6*, *IL-8*, *TNFA*, *IFNB1*, *CCL3* and *LTA*. $^{**}P < 0.01$ and $^{***}P < 0.001$.

ing anti-miR-589-5p (**Figure 5E**). These results suggested that the repression of miR-589-5p could activate the TRAF6 downstream signaling and induce the expression of NF-kB target genes in the condition without LPS treatment.

miR-589-5p and LPS coordinately regulated the TRAF6 downstream signaling

It is well known that LPS can trigger TLR4/NF-kB signaling and induce the expression of NF-kB target genes [2-7]. To evaluate if this was consistent in our system, we treated THP-1 cells with different concentrations of LPS (0, 100, 200 and 400 ng/mL), followed by examining the mRNA levels of *TRAF6* and NF-kB targets, as well as protein levels of TLR4/NF-kB signaling members. The qRT-PCR results indicated that LPS treatments could induce the mRNA levels of *TRAF6* and NF-kB targets (*IL-1B*, *IL-6*, *IL-8* and *TNFA*) in a dose-dependent man-

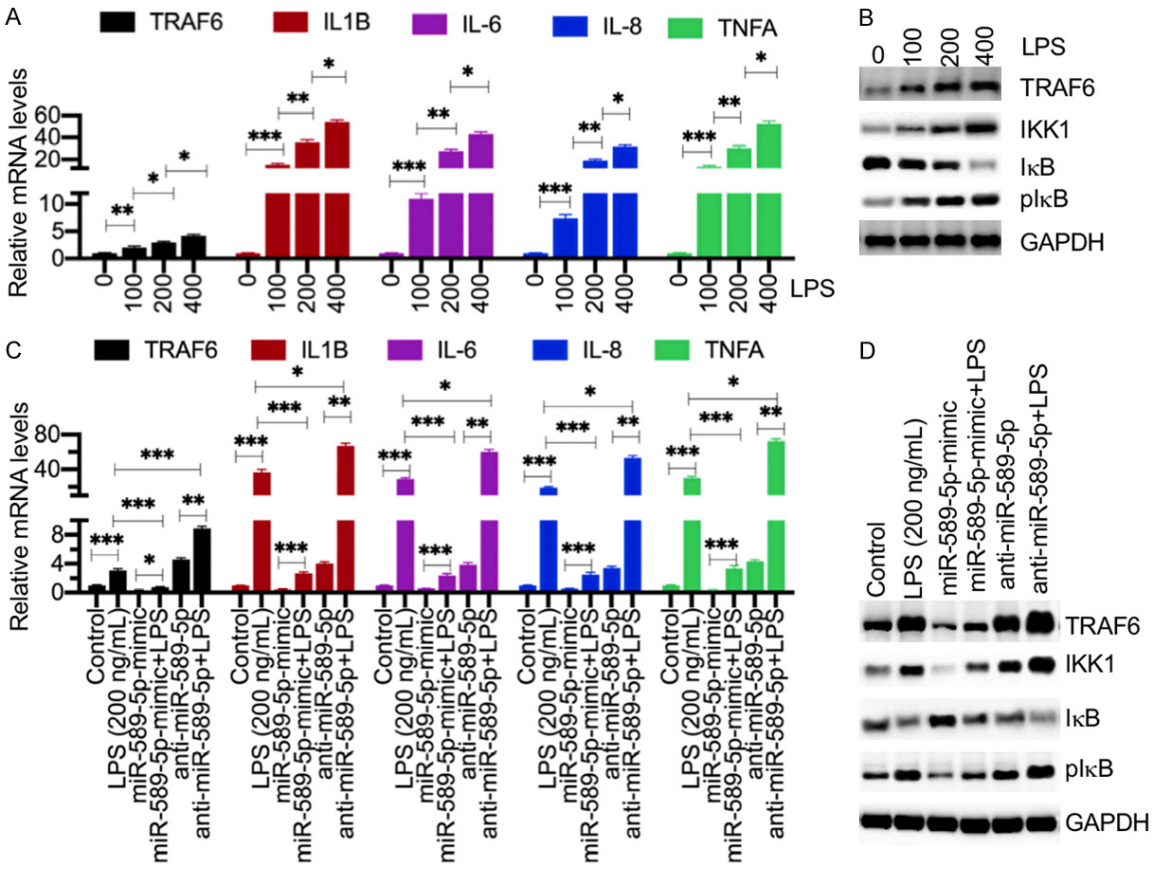

Figure 6. miR-589-5p and TLR4 signaling coregulated the expression of *TRAF6*. (A) LPS induced the expression of *TRAF6* and NF-kB targets. The THP-1 cells were treated with different concentrations of LPS (0, 100, 200 and 400 ng/mL) for 6 h. The resulting cells were used to determine mRNA levels of *TRAF6*, *IL-1B*, *IL-6*, *IL-8* and *TNFA*. $*P < 0.05$, $**P < 0.01$ and $***P < 0.001$. (B) LPS activated TLR4 downstream signaling. Cells used in (A) were subjected to examine the protein levels of TRAF6, IKK1, IkB, and pIkB. GAPDH was a loading control. (C) LPS and miR-589-5p coregulated the expression of *TRAF6* and NF-kB targets. The THP-1 cells were transfected with miR-589-5p-mimic and anti-miR-589 respectively and then treated with 200 ng/mL LPS for 6 h. The resulting cells were used to determine mRNA levels of *TRAF6*, *IL-1B*, *IL-6*, *IL-8* and *TNFA*. $*P < 0.05$, $**P < 0.01$ and $***P < 0.001$. (D) LPS and miR-589-5p coregulated TRAF6 downstream signaling. Cells used in (C) were subjected to examine protein levels of TRAF6, IKK1, IκB, and pIκB. GAPDH was a loading control.

ner (**Figure 6A**). The western blotting results showed that LPS treatments activated the TLR4/NF-kB signaling and caused the accumulation of TRAF6, IKK1 and pIkB but the decrease of IkB protein levels (**Figures 6B** and S4A). These results suggested that LPS could activate the TLR4/NF-kB signaling in THP-1 cells and caused the upregulation of NF-kB targets. Thus, we next sought to evaluate the combined effects of LPS and miR-589-5p. Accordingly, we transfected THP-1 cells with miR-589-5p-mimic and anti-miR-589-5p, respectively, followed by treated with 200 ng/mL LPS. The resulting cells were subjected to evaluate the expression of *TRAF6* and NF-kB targets. The qRT-PCR results indicated that either anti-miR-589-5p or LPS alone could increase the expression of *TRAF6* and NF-kB targets, and their combined treatments caused a much higher induction in *TRAF6* and NF-kB target expression levels than anti-miR-589-5p transfection or LPS treatment alone (**Figure 6C**). The similar patterns of TRAF6, IKK1 and pIkB protein levels were also observed (**Figures 6D** and S4B). These results suggested that miR-589-5p and LPS could coordinately regulate the TRAF6 downstream signaling, affecting the expression of NF-kB targets.

DNA hypermethylation in the promoter of miR-589-5p was responsible for its downregulation

Emerging evidence has shown that DNA methylation and histone acetylation in the promoter

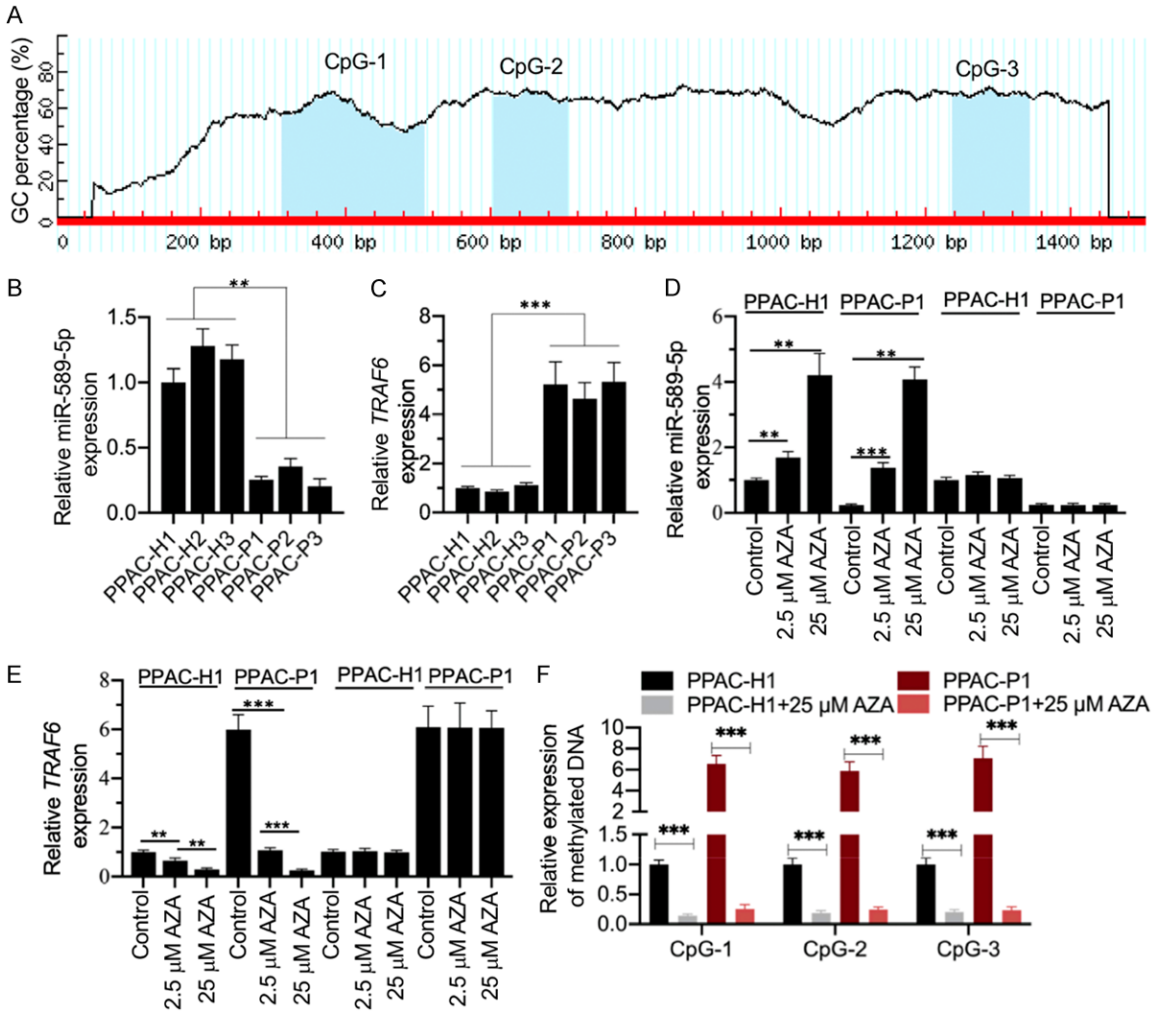

Figure 7. The three CpG islands in the promoter of miR-589-5p were hypermethylated in PPAC cells from SAP tissues. (A) The promoter of miR-589-5p contained three CpG islands. (A) 1500-bp region of the promoter of miR-589-5p was predicted to contain CpG island in a database (http://www.urogene.org). Three CpG islands were identified and indicated as CpG-1, CpG-2 and CpG-3. (B) The relative level of miR-589-5p in PPAC cells. PPAC cells were isolated from the early-stage (0) of pancreatic patients (PPAC-H) and SAP patients (PPAC-P) and miRNAs were isolated to measure miR-589-5p levels. $^{**}P < 0.01$. (C) Relative levels of *TRAF6* in PPAC cells. Total RNA was isolated from the cells used in (B) to measure the expression of *TRAF6*. $^{***}P < 0.001$. (D) AZA treatment increased miR-589-5p levels. The PPAC-H1 and PPAC-P1 cells were treated with different concentrations of AZA (0, 2.5 and 25 mM) and TSA (0, 25 and 250 nM), respectively. MiRNAs were isolated from the cells to examine the expression of miR-589-5p. $^{**}P < 0.01$. (E) AZA treatment decreased *TRAF6* levels. Total RNA was isolated from the cells used in (D), followed by measuring the expression of *TRAF6*. $^{**}P < 0.01$ and $^{***}P < 0.001$. (F) AZA treatment decreased the methylation of CpG islands. The PPAC-H1 and PPAC-P1 cells were treated with or without 25 mM AZA. The genomic DNA from these cells was treated with sodium bisulfite, and then the methylated DNA was determined by qMSP analysis. $^{***}P < 0.001$.

regions of miRNAs are the two primary mechanisms that cause miRNA dysregulation [32, 33]. Thus, we next sought to investigate whether DNA methylation and histone acetylation were involved in the downregulation of miR-589-5p. We primarily analyzed a 1500-bp length of the miR-589-5p promoter. After predicting the CpG islands in a database (http://www.urogene.org), we identified three CpG islands in the promoter of miR-589-5p (**Figure 7A**). These three CpG islands locate in the [-160-(-)262] (CpG-3), [-795-(-)890] (CpG-2), and [-990-(-)1190] (CpG-1). The existence of these CpG islands implied that DNA methylation might be the dominant factor contributing to the downregulation of miR-589-5p because DNA meth-

ylation usually occurs in CpG-rich regions. To verify this hypothesis, we treated PPAC cells with different concentrations of AZA, a DNA methylation inhibitor, followed by detection of miR-589-5p and *TRAF6* mRNA levels. Initially, we measured miR-589-5p and *TRAF6* mRNA in PPAC cells without any treatment to monitor whether PPAC-P cells from SAP patients had lower miR-589-5p but higher *TRAF6* mRNA levels compared to PPAC-H cells from controls. Consistent with the *in vivo* results, we observed that the miR-589-5p level decreased to ~0.4-fold, but the *TRAF6* mRNA level increased to ~5.4-fold in PPAC-P cells compared to PPAC-H cells (**Figure 7B** and **7C**). After AZA treatments, the expression of miR-589-5p increased in a dose-dependent manner in both PPAC-H1 and PPAC-P1 cells (**Figure 7D**). There was no significant difference in miR-589-5p levels in PPAC-H1 and PPAC-P1 cells treated with 25 mM AZA (**Figure 7D**). In contrast, AZA treatment caused the repression of *TRAF6* in a dose-dependent manner, and there was no difference in the expression of *TRAF6* in both cell backgrounds when the AZA concentration was 25 mM (**Figure 7E**). We also treated cells with TSA, an inhibitor of histone deacetylase (HDAC). TSA treatment did not change either miR-589-5p or *TRAF6* levels (**Figure 7D** and **7E**). These results clearly suggested that DNA methylation in the promoter of miR-589-5p caused its downregulation. To further verify that the three CpG islands were hypermethylated, we measured the relative methylated DNA levels using the qMSP method. Our results showed that the methylated DNA levels in the three CpG islands were significantly higher (~6.1-7.0-fold) in PPAC-P1 cells compared to PPAC-H1 cells (**Figure 7F**). After AZA treatment, the methylated DNA levels in the three CpG islands were dramatically decreased in both PPAC-H1 and PPAC-P1 cells (**Figure 7F**). These results suggested that all three CpG islands were hypermethylated in the pancreatic tissues.

AZA treatment inhibited TRAF6 downstream signaling

Since AZA treatment was able to decrease *TRAF6* mRNA level, we speculated that it could also affect TRAF6 downstream signaling. For this purpose, we primarily examined the protein levels of TLR4, TRAF6, IKK1, IkB and pIkB in both PPAC-H1 and PPAC-P1 cells treated with or without AZA. The immunoblot results showed that the protein levels of TRAF6, IKK1 and pIkB were markedly decreased in an AZA dose-dependent manner (**Figures 8A** and S5A), while the IkB protein level was upregulated with the increase of AZA concentrations (**Figures 8A** and S5A). As expected, AZA treatment did not change TLR4 protein levels (**Figures 8A** and S5A). Moreover, we also detected NF-kB subunits in the total, cytoplasmic and nuclear fractions in cells treated with different concentrations of AZA. Our results showed that the protein levels of NF-kB subunits in total cell extracts were not changed (**Figures 8B** and S5B). In the cytoplasmic and nuclear fractions, we observed a dose-dependent increase and decrease in all NF-kB subunits in both cell backgrounds, respectively (**Figures 8C** and S5C). In addition, we also found that AZA treatment could repress the expression of NF-kB downstream targets, including *IL1B*, *IL-6*, *IL-8*, *TNFA*, *IFNB1*, *CCL3* and *LTA*, in a dose-dependent manner (**Figure 8E**).

Discussion

Inflammation is closely associated with the pathogenesis of multiple diseases including SAP [34, 35]. The TLR4/NF-kB pathway plays a dominant role in the regulation of proinflammatory cytokines [36]. In the present study, we verified the increased proinflammatory cytokine levels and the activation of the TLR4/NF-kB pathway in both blood samples and pancreatic samples from SAP patients. Using different strategies such as microarray, bioinformatics and *in vitro* overexpression analyses, we found that miR-589-5p is downregulated in SAP tissues and it can directly target *TRAF6*, an important member of the TLR4/NF-kB pathway. Subsequent mechanistic studies revealed that *TRAF6* was regulated by two-layer mechanisms, including miR-589-5p-mediating repression at the transcriptional level and TLR4-mediated signaling activation at the protein level. These two regulatory mechanisms coordinately caused the significant overexpression of *TRAF6* and the activation of its downstream signaling, leading to the degradation of IkB and the release of NF-kB subunits. The activated NF-kB subunits translocated from the cytoplasm to the nucleus, where they induced the expression of proinflammatory cytokine genes such as *IL-1B*, *IL-6*, *IL-8*, *TNFA*, *IFNB1*, *CCL3* and *LTA*.

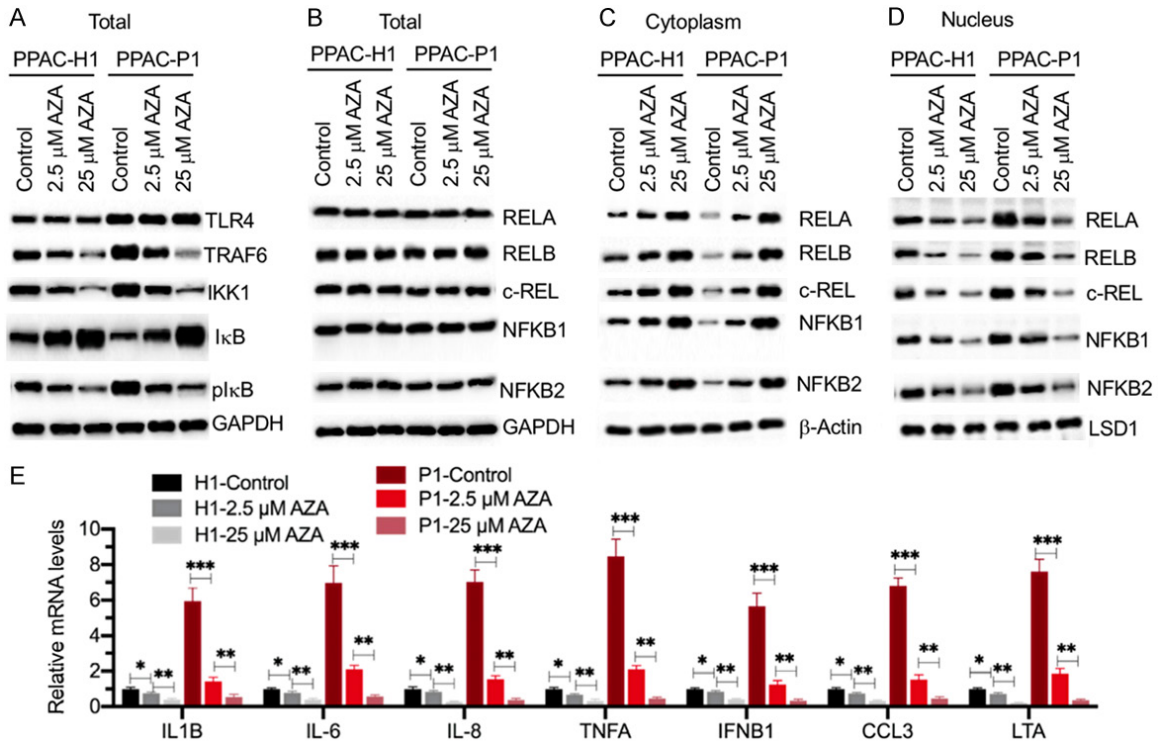

Figure 8. AZA treatment affected TRAF6 downstream signaling. (A) AZA treatment affected the protein levels of TRAF6 downstream members. Total cell extracts from PPAC cells transfected with different concentrations of AZA (0, 2.5 and 25 mM) were subjected to immunoblot analyses to examine the protein levels of TLR4, TRAF6, IKK1, IkB and pIkB. GAPDH was used as a loading control. (B) AZA treatment had no effect on NF-kB subunit protein levels in total extracts. The same cell extracts used in (A) were subjected to immunoblot analyses to examine the protein levels of RELA, RELB, c-REL, NFKB1 and NFKB2. GAPDH was used as a loading control. (C) The protein levels of NF-kB subunits in cytoplasmic fractions. The cytoplasmic fractions from PPAC cells treated with different concentrations of AZA (0, 2.5 and 25 mM) were subjected to immunoblot analyses to examine NF-kB subunit protein levels. β-Actin was used as a loading control. (D) The protein levels of NF-kB subunits in nuclear fractions were significantly decreased after AZA treatment. The nuclear fractions from PPAC cells treated with different concentrations of AZA (0, 2.5 and 25 mM) were subjected to immunoblot analyses to examine NF-kB subunit protein levels. LSD1 was used as a loading control. (E) AZA treatment decreased the expression of NF-kB targets. The cells used in (A) were used for RNA isolation and qRT-PCR analyses to measure the expression of NF-kB targets, including *IL-1B*, *IL-6*, *IL-8*, *TNFA*, *IFNB1*, *CCL3* and *LTA*. $^{**}P < 0.01$ and $^{***}P < 0.001$.

The increased proinflammatory cytokine levels resulted in inflammation and caused the occurrence of SAP (**Figure 9**).

The activation of NF-kB has been observed in pancreatic animal models and pancreatitis patients for many years [37, 38]. Current views recognize that NF-κB activation is an early and critical step in the progression of inflammation [38]. NF-κB plays a central role in linking initial acinar injury to systemic inflammation in the pathogenesis of pancreatitis [39]. The activation of NF-κB signaling has been shown to increase the production of multiple cytokines, such as TNF-α, IL-1β, IL-6 and IL-18, and some chemokines, such as IL-8, MIP1 (macrophage inflammatory protein 1) and MCP1 (monocyte chemoattractant protein 1) [37-39]. In our study, we also verified the activation of NF-κB and the elevated levels of proinflammatory cytokines, including TNF-α, IL-1β, IL-6, IL-15 and IL-18. Many factors and stimuli, such as LPS [40], recombinant TNF-α and IL-6 [41, 42], can activate NF-κB signaling. In the current study, we did not focus on revealing the mechanism underlying TLR4/NF-κB activation but instead on identifying miRNAs that might be involved in the regulation of this pathway. Given that many strategies have attempted to inhibit NF-κB activation from treating inflammatory diseases including cancer [43, 44], using inhibitors to block NF-κB activity or inhibit TLR4/NF-κB signaling may also be effective in the treatment of SAP.

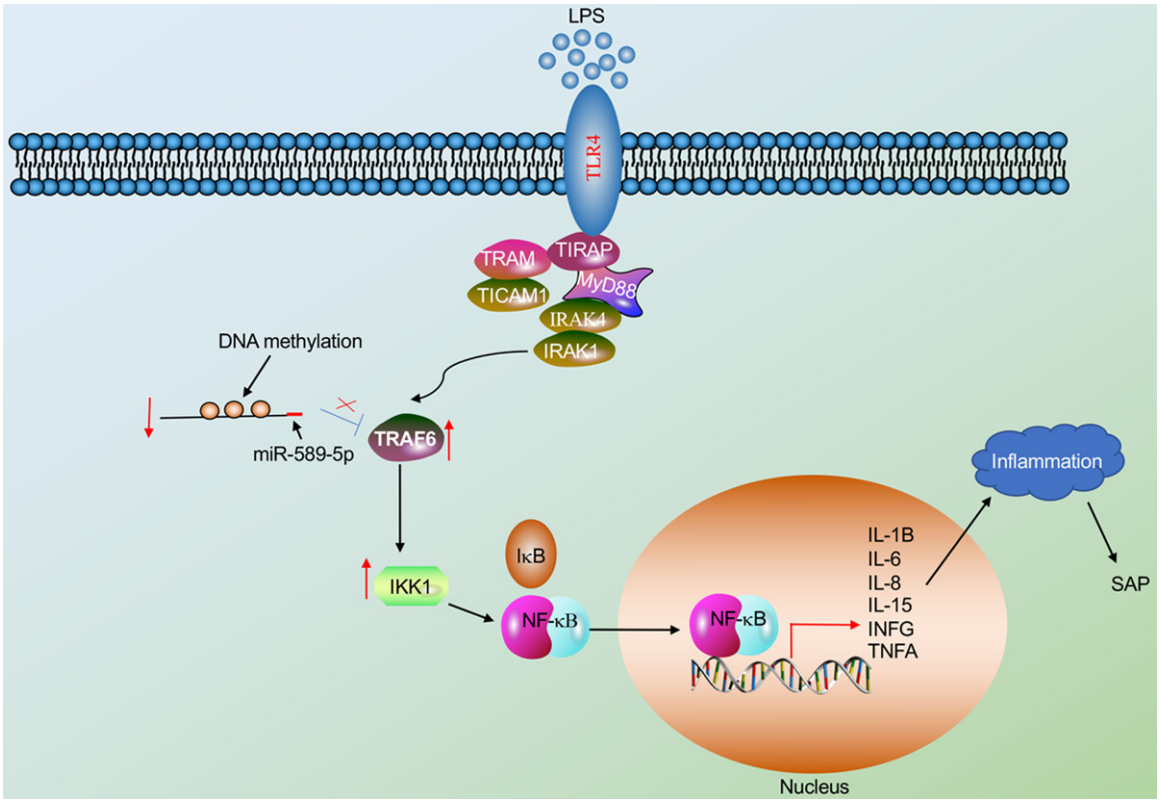

Figure 9. A schematic model of miR-589-5p and TLR4/NF-κB signaling in the pathogenesis of SAP. LPS or other harmful stimuli activates the TLR4, which recruits its downstream adaptors, including TIRAP, TRAM, TICAM1 and MyD88. MyD88 activates a kinase cascade of IRAK4 and IRAK1, activating TRAF6 and IKK1. The activated IKK1 phosphorylates IκB and causes its degradation, leading to the disassociation of IκB/NF-κB. The released NF-κB translocate into the nucleus, where they activate the expression of proinflammatory cytokine genes, including *IL-1B*, *IL-6*, *IL-8*, *IL-15*, *IFNG* and *TNFA*. The maturation and secretion of these proinflammatory cytokines cause inflammation, triggering the occurrence of SAP. On the other hand, miR-589-5p is also involved in the regulation of *TRAF6* at the transcriptional level. The CpG islands in the promoter of miR-589-5p are hypermethylated in SAP samples, causing the downregulation of miR-589-5p. The decreased miR-589-5p attenuates its inhibitory effect on *TRAF6*, leading to the upregulation of *TRAF6*. These two-layer mechanisms coactivate the downstream events.

As in many other diseases, the pathological roles of miRNAs in pancreatitis have also received increasing attention [26]. In the current study, we identified a total of 50 differentially expressed miRNAs in the SAP patients. In this study, we only focused on miR-589-5p, which was significantly decreased in the pancreatic tissues. Our subsequent *in vitro* studies solved three major questions: (1) verified that *TRAF6* was a direct target of miR-589-5p; (2) identified that miR-589-5p and TLR4 signaling could coordinately regulate the expression of *TRAF6*; and (3) revealed DNA hypermethylation of three CpG islands in the promoter of miR-589-5p as the cause leading to its downregulation in SAP patients. Comparing the differentially expressed miRNAs in our microarray results with the published miRNAs involved in the pathology of pancreatitis [26], we found two overlapping miRNAs, miR-21 and miR-122b. However, the functions and targets of these two miRNAs have not been revealed. The other 48 unique miRNAs have not been previously reported to be involved in the pathogenesis of pancreatitis. Thus, our results provide valuable information for future studies in this field. In addition, several studies in different cells and diseases have demonstrated the complicated functions of miR-589. For instance, Zhang and colleagues found that miR-589 can regulate epithelial-mesenchymal transition (EMT) in human peritoneal mesothelial cells isolated from continuous ambulatory peritoneal dialysis (CAPD) patients [45]. Zhang and colleagues identified that miR-589-5p was able to inhibit *MAP3K8* expression and suppress the stemness characteristics

of $CD90^+$ cancer stem cells in hepatocellular carcinoma [46]. In the peritoneal dialysis (PD) patients, the expression of miR-589 was consistently significantly related to peritoneal transport [47]. Long and colleagues found that miR-589-5p could promote cancer stem cell characteristics and chemoresistance by targeting *SOCS2* (suppressor of cytokine signaling 2), *SOCS5*, *PTPN1* (protein tyrosine phosphatase nonreceptor type 1) and *PTPN11*, eventually resulting in the activation of STAT3 (signal transducer and activator of transcription 3) signaling [48]. Liu and colleagues found that the downregulation of miR-589-5p promoted malignancy in human non-small cell lung cancer by targeting *HDAC5* [49]. Consistent with our observation, some studies also found hypermethylation in the promoter of miR-589-5p through bisulfite DNA sequencing [49]. Although we only focused our studies on revealing the function of miR-589-5p, we speculate that the other miRNAs may also be important for the pathogenesis of SAP. When we predicted the target genes of these miRNAs in a database, we found that some miRNAs could target a variety of important genes involved in inflammation. For example, miR-30a-3p is capable of targeting *IL-1B*, miR-150-5p can target *TNFA*, and miR-1323 can target *IL-6*. We are currently evaluating the contributions of these miRNAs in the pathogenesis of SAP and verifying their targets. We speculate that it is likely that multiple miRNAs contribute to the pathology of SAP through regulating the expression of their target genes.

Taken together, our results reveal that both the downregulation of miR-589-5p and the activation of TLR4 signaling contribute to the overexpression of *TRAF6* in the pathogenesis of SAP. The overexpressed TRAF6 triggers its downstream events including the activation of NF-kB, which induces the expression of proinflammatory cytokines, leading to inflammatory response and causing SAP.

Acknowledgements

This study was supported by a grant from Medical Scientific Research of Jiangxi Province, China (No: 2018A136).

Disclosure of conflict of interest

None.

Address correspondence to: Jun Wang, Department of General Surgery, Jiangxi Provincial People's Hospital Affiliated to Nanchang University, Nanchang, Jiangxi, China. E-mail: wangjun981171@163.com

References

[1] Zerem E. Treatment of severe acute pancreatitis and its complications. World J Gastroenterol 2014; 20: 13879-13892.

[2] Weber A, Carbonnel F, Simon N, Kantelip B, Coaquette A, Mantion G, Miguet JP and Di Martino V. Severe acute pancreatitis related to the use of adefovir in a liver transplant recipient. Gastroenterol Clin Biol 2008; 32: 247-249.

[3] Kang R, Lotze MT, Zeh HJ, Billiar TR and Tang D. Cell death and DAMPs in acute pancreatitis. Mol Med 2014; 20: 466-477.

[4] Gu H, Werner J, Bergmann F, Whitcomb DC, Buchler MW and Fortunato F. Necro-inflammatory response of pancreatic acinar cells in the pathogenesis of acute alcoholic pancreatitis. Cell Death Dis 2013; 4: e816.

[5] Liu T, Zhang L, Joo D and Sun SC. NF-kappaB signaling in inflammation. Signal Transduct Target Ther 2017; 2: 17023.

[6] Moudgil KD and Choubey D. Cytokines in autoimmunity: role in induction, regulation, and treatment. J Interferon Cytokine Res 2011; 31: 695-703.

[7] Strober W and Fuss IJ. Proinflammatory cytokines in the pathogenesis of inflammatory bowel diseases. Gastroenterology 2011; 140: 1756-1767.

[8] Turner MD, Nedjai B, Hurst T and Pennington DJ. Cytokines and chemokines: at the crossroads of cell signalling and inflammatory disease. Biochim Biophys Acta 2014; 1843: 2563-2582.

[9] Li G, Wu X, Yang L, He Y, Liu Y, Jin X and Yuan H. TLR4-mediated NF-kappaB signaling pathway mediates HMGB1-induced pancreatic injury in mice with severe acute pancreatitis. Int J Mol Med 2016; 37: 99-107.

[10] Silverman N and Maniatis T. NF-kappaB signaling pathways in mammalian and insect innate immunity. Genes Dev 2001; 15: 2321-2342.

[11] Verstak B, Stack J, Ve T, Mangan M, Hjerrild K, Jeon J, Stahl R, Latz E, Gay N, Kobe B, Bowie AG and Mansell A. The TLR signaling adaptor TRAM interacts with TRAF6 to mediate activation of the inflammatory response by TLR4. J Leukoc Biol 2014; 96: 427-436.

[12] Chen L, Chen Y, Yun H and Jianli Z. Tetramethylpyrazine (TMP) protects rats against acute pancreatitis through NF-kappaB pathway. Bioengineered 2019; 10: 172-181.

[13] Huang H, Liu Y, Daniluk J, Gaiser S, Chu J, Wang H, Li ZS, Logsdon CD and Ji B. Activation of nuclear factor-kappaB in acinar cells in-

creases the severity of pancreatitis in mice. Gastroenterology 2013; 144: 202-210.
[14] Wrzesinski SH, Wan YY and Flavell RA. Transforming growth factor-beta and the immune response: implications for anticancer therapy. Clin Cancer Res 2007; 13: 5262-5270.
[15] Hahm KB, Im YH, Lee C, Parks WT, Bang YJ, Green JE and Kim SJ. Loss of TGF-beta signaling contributes to autoimmune pancreatitis. J Clin Invest 2000; 105: 1057-1065.
[16] Halbrook CJ, Wen HJ, Ruggeri JM, Takeuchi KK, Zhang Y, di Magliano MP and Crawford HC. Mitogen-activated protein kinase kinase activity maintains acinar-to-ductal metaplasia and is required for organ regeneration in pancreatitis. Cell Mol Gastroenterol Hepatol 2017; 3: 99-118.
[17] Irrera N, Bitto A, Interdonato M, Squadrito F and Altavilla D. Evidence for a role of mitogen-activated protein kinases in the treatment of experimental acute pancreatitis. World J Gastroenterol 2014; 20: 16535-16543.
[18] Cao MH, Xu J, Cai HD, Lv ZW, Feng YJ, Li K, Chen CQ and Li YY. p38 MAPK inhibition alleviates experimental acute pancreatitis in mice. Hepatobiliary Pancreat Dis Int 2015; 14: 101-106.
[19] Komar HM, Serpa G, Kerscher C, Schwoegl E, Mace TA, Jin M, Yang MC, Chen CS, Bloomston M, Ostrowski MC, Hart PA, Conwell DL and Lesinski GB. Inhibition of Jak/STAT signaling reduces the activation of pancreatic stellate cells in vitro and limits caerulein-induced chronic pancreatitis in vivo. Sci Rep 2017; 7: 1787.
[20] Wahid F, Shehzad A, Khan T and Kim YY. MicroRNAs: synthesis, mechanism, function, and recent clinical trials. Biochim Biophys Acta 2010; 1803: 1231-1243.
[21] Hammond SM. An overview of microRNAs. Adv Drug Deliv Rev 2015; 87: 3-14.
[22] Gebert LFR and MacRae IJ. Regulation of microRNA function in animals. Nat Rev Mol Cell Biol 2019; 20: 21-37.
[23] O'Brien J, Hayder H, Zayed Y and Peng C. Overview of MicroRNA biogenesis, mechanisms of actions, and circulation. Front Endocrinol (Lausanne) 2018; 9: 402.
[24] Ardekani AM and Naeini MM. The role of MicroRNAs in human diseases. Avicenna J Med Biotechnol 2010; 2: 161-179.
[25] Li Y and Kowdley KV. MicroRNAs in common human diseases. Genomics Proteomics Bioinformatics 2012; 10: 246-253.
[26] Xiang H, Tao X, Xia S, Qu J, Song H, Liu J and Shang D. Targeting MicroRNA Function in Acute Pancreatitis. Front Physiol 2017; 8: 726.
[27] Liu P, Xia L, Zhang WL, Ke HJ, Su T, Deng LB, Chen YX and Lv NH. Identification of serum microRNAs as diagnostic and prognostic biomarkers for acute pancreatitis. Pancreatology 2014; 14: 159-166.
[28] Kusnierz-Cabala B, Nowak E, Sporek M, Kowalik A, Kuzniewski M, Enguita FJ and Stepien E. Serum levels of unique miR-551-5p and endothelial-specific miR-126a-5p allow discrimination of patients in the early phase of acute pancreatitis. Pancreatology 2015; 15: 344-351.
[29] An F, Zhan Q, Xia M, Jiang L, Lu G, Huang M, Guo J and Liu S. From moderately severe to severe hypertriglyceridemia induced acute pancreatitis: circulating miRNAs play role as potential biomarkers. PLoS One 2014; 9: e111058.
[30] Vilmann P and Saftoiu A. Endoscopic ultrasound-guided fine needle aspiration biopsy: equipment and technique. J Gastroenterol Hepatol 2006; 21: 1646-1655.
[31] Gout J, Pommier RM, Vincent DF, Kaniewski B, Martel S, Valcourt U and Bartholin L. Isolation and culture of mouse primary pancreatic acinar cells. J Vis Exp 2013; 78: 50514.
[32] Barter MJ, Bui C and Young DA. Epigenetic mechanisms in cartilage and osteoarthritis: DNA methylation, histone modifications and microRNAs. Osteoarthritis Cartilage 2012; 20: 339-349.
[33] Saito Y, Saito H, Liang G and Friedman JM. Epigenetic alterations and microRNA misexpression in cancer and autoimmune diseases: a critical review. Clin Rev Allergy Immunol 2014; 47: 128-135.
[34] Hunter P. The inflammation theory of disease. The growing realization that chronic inflammation is crucial in many diseases opens new avenues for treatment. EMBO Rep 2012; 13: 968-970.
[35] Kylanpaa L, Rakonczay Z Jr and O'Reilly DA. The clinical course of acute pancreatitis and the inflammatory mediators that drive it. Int J Inflam 2012; 2012: 360685.
[36] Lawrence T. The nuclear factor NF-kappaB pathway in inflammation. Cold Spring Harb Perspect Biol 2009; 1: a001651.
[37] Algul H, Tando Y, Schneider G, Weidenbach H, Adler G and Schmid RM. Acute experimental pancreatitis and NF-kappaB/Rel activation. Pancreatology 2002; 2: 503-509.
[38] Jakkampudi A, Jangala R, Reddy BR, Mitnala S, Nageshwar Reddy D and Talukdar R. NF-kappaB in acute pancreatitis: mechanisms and therapeutic potential. Pancreatology 2016; 16: 477-488.
[39] Sah RP, Dawra RK and Saluja AK. New insights into the pathogenesis of pancreatitis. Curr Opin Gastroenterol 2013; 29: 523-530.
[40] Andreakos E, Sacre SM, Smith C, Lundberg A, Kiriakidis S, Stonehouse T, Monaco C, Feldmann M and Foxwell BM. Distinct pathways of LPS-induced NF-kappa B activation and cyto-

kine production in human myeloid and nonmyeloid cells defined by selective utilization of MyD88 and Mal/TIRAP. Blood 2004; 103: 2229-2237.
[41] Martin AG and Fresno M. Tumor necrosis factor-alpha activation of NF-kappa B requires the phosphorylation of Ser-471 in the transactivation domain of c-Rel. J Biol Chem 2000; 275: 24383-24391.
[42] Wang L, Walia B, Evans J, Gewirtz AT, Merlin D and Sitaraman SV. IL-6 induces NF-kappa B activation in the intestinal epithelia. J Immunol 2003; 171: 3194-3201.
[43] Erstad DJ and Cusack JC Jr. Targeting the NF-kappaB pathway in cancer therapy. Surg Oncol Clin N Am 2013; 22: 705-746.
[44] Liou GY and Storz P. Inflammatory macrophages in pancreatic acinar cell metaplasia and initiation of pancreatic cancer. Oncoscience 2015; 2: 247-251.
[45] Zhang K, Zhang H, Zhou X, Tang WB, Xiao L, Liu YH, Liu H, Peng YM, Sun L and Liu FY. miRNA589 regulates epithelial-mesenchymal transition in human peritoneal mesothelial cells. J Biomed Biotechnol 2012; 2012: 673096.
[46] Zhang X, Jiang P, Shuai L, Chen K, Li Z, Zhang Y, Jiang Y and Li X. miR-589-5p inhibits MAP3K8 and suppresses CD90(+) cancer stem cells in hepatocellular carcinoma. J Exp Clin Cancer Res 2016; 35: 176.
[47] Szeto CC, Chow KM, Kwan BC, Cheng PM, Luk CC, Ng JK, Law MC, Leung CB and Li PK. Peritoneal dialysis effluent miR-21 and miR-589 levels correlate with longitudinal change in peritoneal transport characteristics. Clin Chim Acta 2017; 464: 106-112.
[48] Long J, Jiang C, Liu B, Dai Q, Hua R, Chen C, Zhang B and Li H. Maintenance of stemness by miR-589-5p in hepatocellular carcinoma cells promotes chemoresistance via STAT3 signaling. Cancer Lett 2018; 423: 113-126.
[49] Liu C, Lv D, Li M, Zhang X, Sun G, Bai Y and Chang D. Hypermethylation of miRNA-589 promoter leads to upregulation of HDAC5 which promotes malignancy in non-small cell lung cancer. Int J Oncol 2017; 50: 2079-2090.

Table S1. The basic information of healthy controls (HC, n=48) and acute pancreatitis patients (AP, n=48)

Parameters	HC	AP
Mean age	46.3±5.8	44.6±6.4
Gender	24 M/24 F	24 M/24 F

F: female; M: male.

Table S2. The basic information of pancreatic cancer patients (Control, n=24) and acute pancreatitis patients (AP, n=24)

Parameters	Control	AP
Mean age	62.5±6.8	55.2±4.9
Gender	15 M/9 F	11 M/13 F
Cancer stage	0	NA

F: female; M: male.

Table S3. Primers used for qRT-PCR analyzes

Gene	Forward Primers	Reverse primers
TRAF6	5'-GTGACAACTGTGCTGCATCAATG-3'	5'-ACTATGAACAGCCTGGGCCAACA-3'
IL1B	5'-TCTCCGACCACCACTACAGCAAG-3'	5'-CTGGAGGTGGAGAGCTTTCAGT-3'
IL-6	5'-ACCTAGAGTACCTCCAGAACAGA-3'	5'-AGATGAGTTGTCATGTCCTGCA-3'
IL-8	5'-TGACTTCCAAGCTGGCCGTGGC-3'	5'-CTTCTCCACAACCCTCTGCACCC-3'
TNFA	5'-AGGGCTCCAGGCGGTGCTTGT-3'	5'-GGTACAGGCCCTCTGATGGCAC-3'
IFNB1	5'-GAAGCTCCTGTGGCAATTGAAT-3'	5'-CTGATGATAGACATTAGCCA-3'
CCL3	5'-TGTCCTCCTCTGCACCATGGCTCT-3'	5'-CCTCACTGGGGTCAGCACAGA-3'
LTA	5'-TTCAGCTGCCCAGACTGCCCGT-3'	5'-CCACCTGGGAGTAGACGAAGTAG-3'
β-Actin	5'-AGAGCTACGAGCTGCCTGAC-3'	5'-AGCACTGTGTTGGCGTACAG-3'

Table S4. Primers used for qMSP assays

Gene	Forward Primers	Reverse primers
CpG1	5'-GGTTTTAGATAGTAGGAGATGGAAA-3'	5'-ACTTAATTTTTAACCCCAAAAACTC-3'
CpG2	5'-AGGTGTTTAGGATGTGGTAGGTTTA-3'	5'-CCCCTCAAAAAACAAAATAAAAAA-3'
CpG3	5'-TTTTAAGTTTTGTTATTAAAGAGATTT-3'	5'- TTCCTCTAAATTCCTACCTTCTAC-3'

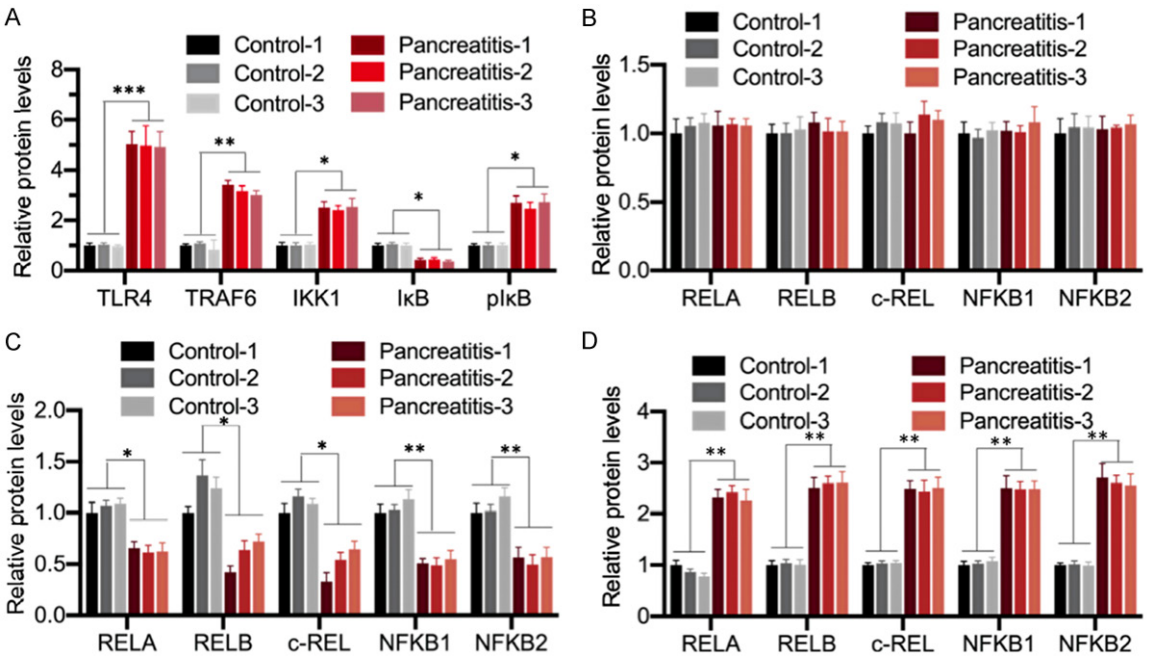

Figure S1. Quantification of the protein levels of members of the TLR4/NF-kB signaling pathway and NF-kB subunits. The protein levels in **Figure 2** were quantified using ImageJ software. The signal intensity of individual proteins was normalized to the loading controls. A. The relative protein levels in **Figure 2A**. *$P < 0.05$, ** $P < 0.01$, and *** $P < 0.001$. B. The relative protein levels in **Figure 2B**. C. The relative protein levels in **Figure 2C**. *$P < 0.05$ and ** $P < 0.01$. D. The relative protein levels in **Figure 2D**. *$P < 0.05$ and ** $P < 0.01$.

Table S5. Differentially expressed miRNAs in pancreatitis patients

miRNA	Average fold change	*P* Value	Expression
miR-let-7e	12.3	0.00054	Up
miR-19b-3p	11.5	0.00051	Up
miR-211-5p	11.1	0.00032	Up
miR-21-5p	10.6	0.00012	Up
miR-127-3p	10.3	0.00057	Up
miR-766-5p	9.8	0.00066	Up
miR-455-3p	9.5	0.00089	Up
miR-219a-5p	9.2	0.00016	Up
miR-544a	8.9	0.00058	Up
miR-411-3p	8.4	0.00025	Up
miR-488-3p	8.1	0.00077	Up
miR-650	7.8	0.00026	Up
miR-579-3p	7.3	0.00047	Up
miR-664a-3p	6.9	0.00087	Up
miR-107	6.7	0.00047	Up
miR-122b-5p	6.4	0.00027	Up
miR-412-5p	5.9	0.00076	Up
miR-487a-5p	5.3	0.00028	Up
miR-552-5p	4.9	0.00021	Up
miR-568	4.2	0.00055	Up
miR-20b-5p	-16.4	0.00069	Down
miR-589-5p	-15.9	0.00018	Down
miR-26a-5p	-15.7	0.00055	Down

miR-124-5p	-15.3	0.00027	Down
miR-194-5p	-14.8	0.00038	Down
miR-892c-5p	-14.3	0.00055	Down
miR-150-5p	-13.7	0.00078	Down
miR-627-3p	-13.4	0.00048	Down
miR-301a-3p	-12.9	0.00068	Down
miR-875-3p	-12.7	0.00037	Down
miR-607	-12.3	0.00069	Down
miR-505-3p	-11.9	0.00013	Down
miR-30a-3p	-11.5	0.00017	Down
miR-205-3p	-11.1	0.00026	Down
miR-330-5p	-10.5	0.00036	Down
miR-149-5p	-10.1	0.00065	Down
miR-519e-5p	-9.6	0.00036	Down
miR-1323	-9.3	0.00085	Down
miR-31-3p	-9.1	0.00081	Down
miR-610	-8.8	0.00066	Down
miR-942-3p	-8.2	0.00043	Down
miR-143-3p	-7.8	0.00024	Down
miR-374b-5p	-7.2	0.00051	Down
miR-1278	-6.7	0.00042	Down
miR-608	-6.1	0.00077	Down
miR-661	-5.4	0.00089	Down
miR-4263	-5.4	0.00032	Down
miR-130b-3p	-4.8	0.00052	Down
miR-454-3p	-4.2	0.00012	Down
miR-650	-3.9	0.00054	Down

Table S6. The candidate target genes of miR-589-5p

There are 451 predicted targets for hsa-miR-589-5p in miRDB.

Target Detail	Target Rank	Target Score	miRNA Name	Gene Symbol	Gene Description
Details	1	99	hsa-miR-589-5p	NPTN	neuroplastin
Details	2	98	hsa-miR-589-5p	VPS13D	vacuolar protein sorting 13 homolog D
Details	3	98	hsa-miR-589-5p	TRAF6	TNF receptor associated factor 6
Details	4	97	hsa-miR-589-5p	IRAK1	interleukin 1 receptor associated kinase 1
Details	5	96	hsa-miR-589-5p	TNRC6A	trinucleotide repeat containing 6A
Details	6	95	hsa-miR-589-5p	PRKAR2A	protein kinase cAMP-dependent type II regulatory subunit alpha
Details	7	95	hsa-miR-589-5p	TMEM237	transmembrane protein 237
Details	8	94	hsa-miR-589-5p	CMTM6	CKLF like MARVEL transmembrane domain containing 6
Details	9	94	hsa-miR-589-5p	SET	SET nuclear proto-oncogene
Details	10	94	hsa-miR-589-5p	DCUN1D2	defective in cullin neddylation 1 domain containing 2
Details	11	94	hsa-miR-589-5p	CAT	catalase
Details	12	94	hsa-miR-589-5p	PPP1R11	protein phosphatase 1 regulatory inhibitor subunit 11
Details	13	93	hsa-miR-589-5p	MED20	mediator complex subunit 20
Details	14	93	hsa-miR-589-5p	TMEM132D	transmembrane protein 132D
Details	15	93	hsa-miR-589-5p	TTC31	tetratricopeptide repeat domain 31
Details	16	93	hsa-miR-589-5p	ZFYVE1	zinc finger FYVE-type containing 1
Details	17	93	hsa-miR-589-5p	MAP3K8	mitogen-activated protein kinase kinase kinase 8
Details	18	93	hsa-miR-589-5p	MAT2A	methionine adenosyltransferase 2A
Details	19	92	hsa-miR-589-5p	ROR1	receptor tyrosine kinase like orphan receptor 1
Details	20	92	hsa-miR-589-5p	HHAT	hedgehog acyltransferase
Details	21	92	hsa-miR-589-5p	TTC17	tetratricopeptide repeat domain 17
Details	22	91	hsa-miR-589-5p	PRC1	protein regulator of cytokinesis 1
Details	23	91	hsa-miR-589-5p	CPLX4	complexin 4
Details	24	90	hsa-miR-589-5p	SGIP1	SH3 domain GRB2 like endophilin interacting protein 1
Details	25	90	hsa-miR-589-5p	SIN3A	SIN3 transcription regulator family member A
Details	26	90	hsa-miR-589-5p	PHOX2B	paired like homeobox 2B
Details	27	90	hsa-miR-589-5p	FTHL17	ferritin heavy chain like 17
Details	28	90	hsa-miR-589-5p	ELAC1	elaC ribonuclease Z 1
Details	29	90	hsa-miR-589-5p	PKN2	protein kinase N2
Details	30	89	hsa-miR-589-5p	SLC12A6	solute carrier family 12 member 6
Details	31	89	hsa-miR-589-5p	PHKB	phosphorylase kinase regulatory subunit beta
Details	32	89	hsa-miR-589-5p	KLF7	Kruppel like factor 7
Details	33	89	hsa-miR-589-5p	RFXAP	regulatory factor X associated protein
Details	34	89	hsa-miR-589-5p	ITGB3	integrin subunit beta 3

Details	35	89	hsa-miR589-5p	BMPR1A	bone morphogenetic protein receptor type 1A
Details	37	89	hsa-miR-589-5p	TRMT9B	tRNA methyltransferase 9B (putative)
Details	38	88	hsa-miR-589-5p	ZNF195	zinc finger protein 195
Details	39	88	hsa-miR-589-5p	DCAF7	DDB1 and CUL4 associated factor 7
Details	40	87	hsa-miR-589-5p	SPRY4	sprouty RTK signaling antagonist 4
Details	41	87	hsa-miR-589-5p	PRICKLE2	prickle planar cell polarity protein 2
Details	42	87	hsa-miR-589-5p	GPATCH2L	G-patch domain containing 2 like
Details	43	87	hsa-miR-589-5p	G3BP1	G3BP stress granule assembly factor 1
Details	44	87	hsa-miR-589-5p	INO80D	INO80 complex subunit D
Details	45	87	hsa-miR-589-5p	BAG1	BCL2 associated athanogene 1
Details	46	86	hsa-miR-589-5p	SLC25A14	solute carrier family 25 member 14
Details	47	86	hsa-miR-589-5p	PURG	purine rich element binding protein G
Details	48	86	hsa-miR-589-5p	BCORL1	BCL6 corepressor like 1
Details	49	86	hsa-miR-589-5p	ANKRD46	ankyrin repeat domain 46
Details	50	86	hsa-miR-589-5p	ETV5	ETS variant 5
Details	51	86	hsa-miR-589-5p	PIAS1	protein inhibitor of activated STAT 1
Details	52	86	hsa-miR-589-5p	VAPB	VAMP associated protein B and C
Details	53	85	hsa-miR-589-5p	FBXL5	F-box and leucine rich repeat protein 5
Details	54	85	hsa-miR-589-5p	LRRC8E	leucine rich repeat containing 8 VRAC subunit E
Details	55	85	hsa-miR-589-5p	UMPS	uridine monophosphate synthetase
Details	56	85	hsa-miR-589-5p	ZC4H2	zinc finger C4H2-type containing
Details	57	85	hsa-miR-589-5p	MGAT5B	alpha-1,6-mannosylglycoprotein 6-beta-N-acetylglucosaminyltransferase B
Details	58	85	hsa-miR-589-5p	TMEM185B	transmembrane protein 185B
Details	59	84	hsa-miR-589-5p	ANKLE2	ankyrin repeat and LEM domain containing 2
Details	60	84	hsa-miR-589-5p	ZBTB22	zinc finger and BTB domain containing 22
Details	61	84	hsa-miR-589-5p	CALCOCO1	calcium binding and coiled-coil domain 1
Details	62	84	hsa-miR-589-5p	PSMD9	proteasome 26S subunit, non-ATPase 9
Details	63	84	hsa-miR-589-5p	ATP23	ATP23 metallopeptidase and ATP synthase assembly factor homolog
Details	64	84	hsa-miR-589-5p	NOVA1	NOVA alternative splicing regulator 1
Details	65	84	hsa-miR-589-5p	MPPE1	metallophosphoesterase 1
Details	66	84	hsa-miR-589-5p	RCAN3	RCAN family member 3
Details	67	83	hsa-miR-589-5p	MYO6	myosin VI
Details	68	83	hsa-miR-589-5p	CALHM5	calcium homeostasis modulator family member 5
Details	69	83	hsa-miR-589-5p	LAT	linker for activation of T cells
Details	70	83	hsa-miR-589-5p	TOX	thymocyte selection associated high mobility group box
Details	71	83	hsa-miR-589-5p	MYT1	myelin transcription factor 1
Details	72	83	hsa-miR-589-5p	SLC3A1	solute carrier family 3 member 1

Details	73	83	hsa-miR-589-5p	PNPLA4	patatin like phospholipase domain containing 4
Details	74	83	hsa-miR-589-5p	SHCBP1	SHC binding and spindle associated 1
Details	75	83	hsa-miR-589-5p	SEH1L	SEH1 like nucleoporin
Details	76	82	hsa-miR-589-5p	AGAP1	ArfGAP with GTPase domain, ankyrin repeat and PH domain 1
Details	77	82	hsa-miR-589-5p	MOCS1	molybdenum cofactor synthesis 1
Details	78	82	hsa-miR-589-5p	TMEM74	transmembrane protein 74
Details	79	82	hsa-miR-589-5p	POLR2G	RNA polymerase II subunit G
Details	80	81	hsa-miR-589-5p	ERRFI1	ERBB receptor feedback inhibitor 1
Details	81	81	hsa-miR-589-5p	CEP170B	centrosomal protein 170B
Details	82	81	hsa-miR-589-5p	SLFN5	schlafen family member 5
Details	83	81	hsa-miR-589-5p	PIP4K2B	phosphatidylinositol-5-phosphate 4-kinase type 2 beta
Details	84	81	hsa-miR-589-5p	ASPH	aspartate beta-hydroxylase
Details	85	80	hsa-miR-589-5p	KCNK5	potassium two pore domain channel subfamily K member 5
Details	86	80	hsa-miR-589-5p	CAVIN1	caveolae associated protein 1
Details	87	80	hsa-miR-589-5p	TRMT6	tRNA methyltransferase 6
Details	88	80	hsa-miR-589-5p	TMEM101	transmembrane protein 101
Details	89	80	hsa-miR-589-5p	DOK5	docking protein 5
Details	90	80	hsa-miR-589-5p	MARVELD3	MARVEL domain containing 3
Details	91	80	hsa-miR-589-5p	RGS5	regulator of G protein signaling 5
Details	92	80	hsa-miR-589-5p	SEMA3G	semaphorin 3G
Details	93	80	hsa-miR-589-5p	ERAL1	Era like 12S mitochondrial rRNA chaperone 1
Details	94	80	hsa-miR-589-5p	OAS2	2'-5'-oligoadenylate synthetase 2
Details	95	79	hsa-miR-589-5p	GOLGA7	golgin A7
Details	96	79	hsa-miR-589-5p	ARMCX5-GPRASP2	ARMCX5-GPRASP2 readthrough
Details	97	79	hsa-miR-589-5p	GPRASP2	G protein-coupled receptor associated sorting protein 2
Details	98	79	hsa-miR-589-5p	CLOCK	clock circadian regulator
Details	99	78	hsa-miR-589-5p	UNC5C	unc-5 netrin receptor C
Details	100	78	hsa-miR-589-5p	CARD10	caspase recruitment domain family member 10
Details	101	78	hsa-miR-589-5p	TRMT1L	tRNA methyltransferase 1 like
Details	102	78	hsa-miR-589-5p	BCLAF3	BCLAF1 and THRAP3 family member 3
Details	103	78	hsa-miR-589-5p	ADGRL2	adhesion G protein-coupled receptor L2
Details	104	78	hsa-miR-589-5p	ARID1B	AT-rich interaction domain 1B
Details	105	78	hsa-miR-589-5p	DGKK	diacylglycerol kinase kappa
Details	106	78	hsa-miR-589-5p	PSMG3	proteasome assembly chaperone 3
Details	107	77	hsa-miR-589-5p	CRADD	CASP2 and RIPK1 domain containing adaptor with death domain
Details	108	77	hsa-miR-589-5p	SALL3	spalt like transcription factor 3
Details	109	77	hsa-miR-589-5p	SNRNP27	small nuclear ribonucleoprotein U4/U6.U5 subunit 27

Details	110	77	hsa-miR-589-5p	RCSD1	RCSD domain containing 1
Details	111	77	hsa-miR-589-5p	FAM107B	family with sequence similarity 107 member B
Details	112	77	hsa-miR-589-5p	SEPHS2	selenophosphate synthetase 2
Details	113	77	hsa-miR-589-5p	GPAT4	glycerol-3-phosphate acyltransferase 4
Details	114	77	hsa-miR-589-5p	THADA	THADA, armadillo repeat containing
Details	115	76	hsa-miR-589-5p	ZHX3	zinc fingers and homeoboxes 3
Details	116	76	hsa-miR-589-5p	TENM1	teneurin transmembrane protein 1
Details	117	76	hsa-miR-589-5p	ZMAT2	zinc finger matrin-type 2
Details	118	76	hsa-miR-589-5p	FAM86B2	family with sequence similarity 86 member B2
Details	119	76	hsa-miR-589-5p	HDX	highly divergent homeobox
Details	120	76	hsa-miR-589-5p	BPY2	basic charge Y-linked 2
Details	121	76	hsa-miR-589-5p	SPRYD7	SPRY domain containing 7
Details	122	76	hsa-miR-589-5p	BPY2B	basic charge Y-linked 2B
Details	123	76	hsa-miR-589-5p	CACNA2D1	calcium voltage-gated channel auxiliary subunit alpha2delta 1
Details	124	76	hsa-miR-589-5p	C14orf132	chromosome 14 open reading frame 132
Details	125	76	hsa-miR-589-5p	SORT1	sortilin 1
Details	126	76	hsa-miR-589-5p	CELF2	CUGBP Elav-like family member 2
Details	127	76	hsa-miR-589-5p	CAMTA1	calmodulin binding transcription activator 1
Details	128	76	hsa-miR-589-5p	BPY2C	basic charge Y-linked 2C
Details	129	75	hsa-miR-589-5p	TTL	tubulin tyrosine ligase
Details	130	75	hsa-miR-589-5p	DLL1	delta like canonical Notch ligand 1
Details	131	75	hsa-miR-589-5p	RELT	RELT, TNF receptor
Details	132	75	hsa-miR-589-5p	NFAT5	nuclear factor of activated T cells 5
Details	133	75	hsa-miR-589-5p	SLC25A38	solute carrier family 25 member 38
Details	134	75	hsa-miR-589-5p	GYPA	glycophorin A (MNS blood group)
Details	135	75	hsa-miR-589-5p	VCPIP1	valosin containing protein interacting protein 1
Details	136	75	hsa-miR-589-5p	EIF4G2	eukaryotic translation initiation factor 4 gamma 2
Details	137	75	hsa-miR-589-5p	GLCE	glucuronic acid epimerase
Details	138	74	hsa-miR-589-5p	DIP2B	disco interacting protein 2 homolog B
Details	139	74	hsa-miR-589-5p	FAM122C	family with sequence similarity 122C
Details	140	74	hsa-miR-589-5p	FZD3	frizzled class receptor 3
Details	141	74	hsa-miR-589-5p	SEMA6A	semaphorin 6A
Details	142	74	hsa-miR-589-5p	RNF4	ring finger protein 4
Details	143	74	hsa-miR-589-5p	SLC25A20	solute carrier family 25 member 20
Details	144	74	hsa-miR-589-5p	BIN2	bridging integrator 2
Details	145	74	hsa-miR-589-5p	TLN2	talin 2
Details	146	74	hsa-miR-589-5p	CTNNA3	catenin alpha 3
Details	147	74	hsa-miR-589-5p	RBPMS2	RNA binding protein, mRNA processing factor 2

Details	148	74	hsa-miR-589-5p	C18orf32	chromosome 18 open reading frame 32
Details	149	74	hsa-miR-589-5p	ZNF501	zinc finger protein 501
Details	150	73	hsa-miR-589-5p	TMEM245	transmembrane protein 245
Details	151	73	hsa-miR-589-5p	CNNM4	cyclin and CBS domain divalent metal cation transport mediator 4
Details	152	73	hsa-miR-589-5p	KRTAP2-3	keratin associated protein 2-3
Details	153	73	hsa-miR-589-5p	MOB3C	MOB kinase activator 3C
Details	154	73	hsa-miR-589-5p	TADA2B	transcriptional adaptor 2B
Details	155	73	hsa-miR-589-5p	ROBO1	roundabout guidance receptor 1
Details	156	73	hsa-miR-589-5p	FAM131C	family with sequence similarity 131 member C
Details	157	73	hsa-miR-589-5p	MMP16	matrix metallopeptidase 16
Details	158	73	hsa-miR-589-5p	LRRC75A	leucine rich repeat containing 75A
Details	159	73	hsa-miR-589-5p	PPM1K	protein phosphatase, Mg2+/Mn2+ dependent 1K
Details	160	73	hsa-miR-589-5p	RPL17-C18orf32	RPL17-C18orf32 readthrough
Details	161	73	hsa-miR-589-5p	JAKMIP3	Janus kinase and microtubule interacting protein 3
Details	162	73	hsa-miR-589-5p	GPR158	G protein-coupled receptor 158
Details	163	73	hsa-miR-589-5p	SBNO1	strawberry notch homolog 1
Details	164	73	hsa-miR-589-5p	SLA2	Src like adaptor 2
Details	165	72	hsa-miR-589-5p	GRIA3	glutamate ionotropic receptor AMPA type subunit 3
Details	166	72	hsa-miR-589-5p	LUC7L	LUC7 like
Details	167	72	hsa-miR-589-5p	PIP5K1B	phosphatidylinositol-4-phosphate 5-kinase type 1 beta
Details	168	72	hsa-miR-589-5p	PLPPR2	phospholipid phosphatase related 2
Details	169	72	hsa-miR-589-5p	CRYM	crystallin mu
Details	170	72	hsa-miR-589-5p	KLHL29	kelch like family member 29
Details	171	72	hsa-miR-589-5p	IFI35	interferon induced protein 35
Details	172	72	hsa-miR-589-5p	LYPLAL1	lysophospholipase like 1
Details	173	72	hsa-miR-589-5p	ZNF250	zinc finger protein 250
Details	174	71	hsa-miR-589-5p	CALR	Calreticulin
Details	175	71	hsa-miR-589-5p	FAM98B	family with sequence similarity 98 member B
Details	176	71	hsa-miR-589-5p	ENDOD1	endonuclease domain containing 1
Details	177	71	hsa-miR-589-5p	ARL8A	ADP ribosylation factor like GTPase 8A
Details	178	71	hsa-miR-589-5p	TXK	TXK tyrosine kinase
Details	179	71	hsa-miR-589-5p	ATP13A3	ATPase 13A3
Details	180	71	hsa-miR-589-5p	NOTCH2	notch 2
Details	181	71	hsa-miR-589-5p	GPT2	glutamic--pyruvic transaminase 2
Details	182	71	hsa-miR-589-5p	MICU1	mitochondrial calcium uptake 1
Details	183	71	hsa-miR-589-5p	GABRA1	gamma-aminobutyric acid type A receptor alpha1 subunit
Details	184	71	hsa-miR-589-5p	UCP3	uncoupling protein 3

Details	185	71	hsa-miR-589-5p	ZRANB3	zinc finger RANBP2-type containing 3
Details	186	71	hsa-miR-589-5p	ATP8B2	ATPase phospholipid transporting 8B2
Details	187	71	hsa-miR-589-5p	MECR	mitochondrial trans-2-enoyl-CoA reductase
Details	188	71	hsa-miR-589-5p	IGF2R	insulin like growth factor 2 receptor
Details	189	71	hsa-miR-589-5p	GUCY1A2	guanylate cyclase 1 soluble subunit alpha 2
Details	190	71	hsa-miR-589-5p	RTN4RL1	reticulon 4 receptor like 1
Details	191	70	hsa-miR-589-5p	ZNHIT3	zinc finger HIT-type containing 3
Details	192	70	hsa-miR-589-5p	FAM199X	family with sequence similarity 199, X-linked
Details	193	70	hsa-miR-589-5p	NDE1	nudE neurodevelopment protein 1
Details	194	70	hsa-miR-589-5p	HDAC5	histone deacetylase 5
Details	195	70	hsa-miR-589-5p	SYT10	synaptotagmin 10
Details	196	70	hsa-miR-589-5p	IYD	iodotyrosine deiodinase
Details	197	70	hsa-miR-589-5p	ZNF473	zinc finger protein 473
Details	198	70	hsa-miR-589-5p	SIRPG	signal regulatory protein gamma
Details	199	70	hsa-miR-589-5p	LUZP1	leucine zipper protein 1
Details	200	69	hsa-miR-589-5p	AMER2	APC membrane recruitment protein 2
Details	201	69	hsa-miR-589-5p	FAM86B1	family with sequence similarity 86 member B1
Details	202	69	hsa-miR-589-5p	ALKBH5	alkB homolog 5, RNA demethylase
Details	203	69	hsa-miR-589-5p	LSM4	LSM4 homolog, U6 small nuclear RNA and mRNA degradation associated
Details	204	69	hsa-miR-589-5p	PRMT3	protein arginine methyltransferase 3
Details	205	69	hsa-miR-589-5p	RNF212	ring finger protein 212
Details	206	69	hsa-miR-589-5p	NUAK2	NUAK family kinase 2
Details	207	69	hsa-miR-589-5p	PTPN5	protein tyrosine phosphatase, non-receptor type 5
Details	208	69	hsa-miR-589-5p	SCN3B	sodium voltage-gated channel beta subunit 3
Details	209	69	hsa-miR-589-5p	KPNA4	karyopherin subunit alpha 4
Details	210	69	hsa-miR-589-5p	TLCD2	TLC domain containing 2
Details	211	69	hsa-miR-589-5p	SOX6	SRY-box 6
Details	212	68	hsa-miR-589-5p	ACOX1	acyl-CoA oxidase 1
Details	213	68	hsa-miR-589-5p	SLC30A8	solute carrier family 30 member 8
Details	214	68	hsa-miR-589-5p	TMEM176B	transmembrane protein 176B
Details	215	68	hsa-miR-589-5p	LRMP	lymphoid restricted membrane protein
Details	216	68	hsa-miR-589-5p	MTR	5-methyltetrahydrofolate-homocysteine methyltransferase
Details	217	67	hsa-miR-589-5p	CNTFR	ciliary neurotrophic factor receptor
Details	218	67	hsa-miR-589-5p	KLHL36	kelch like family member 36
Details	219	67	hsa-miR-589-5p	ACTR8	ARP8 actin related protein 8 homolog
Details	220	67	hsa-miR-589-5p	FAM20B	FAM20B, glycosaminoglycan xylosylkinase
Details	221	67	hsa-miR-589-5p	ABL2	ABL proto-oncogene 2, non-receptor tyrosine kinase

Details	222	67	hsa-miR-589-5p	NUMB	NUMB, endocytic adaptor protein
Details	223	66	hsa-miR-589-5p	RBM25	RNA binding motif protein 25
Details	224	66	hsa-miR-589-5p	HK2	hexokinase 2
Details	225	66	hsa-miR-589-5p	PADI3	peptidyl arginine deiminase 3
Details	226	66	hsa-miR-589-5p	TMC8	transmembrane channel like 8
Details	227	66	hsa-miR-589-5p	ST3GAL1	ST3 beta-galactoside alpha-2,3-sialyltransferase 1
Details	228	66	hsa-miR-589-5p	PROX1	prospero homeobox 1
Details	229	66	hsa-miR-589-5p	SLC18A2	solute carrier family 18 member A2
Details	230	66	hsa-miR-589-5p	ARHGAP29	Rho GTPase activating protein 29
Details	231	66	hsa-miR-589-5p	CNNM1	cyclin and CBS domain divalent metal cation transport mediator 1
Details	232	66	hsa-miR-589-5p	SAMD8	sterile alpha motif domain containing 8
Details	233	66	hsa-miR-589-5p	BABAM1	BRISC and BRCA1 A complex member 1
Details	234	66	hsa-miR-589-5p	YBX1	Y-box binding protein 1
Details	235	66	hsa-miR-589-5p	AASS	aminoadipate-semialdehyde synthase
Details	236	66	hsa-miR-589-5p	MOXD1	monooxygenase DBH like 1
Details	237	66	hsa-miR-589-5p	SLC2A14	solute carrier family 2 member 14
Details	238	65	hsa-miR-589-5p	ADGRG2	adhesion G protein-coupled receptor G2
Details	239	65	hsa-miR-589-5p	DCTN5	dynactin subunit 5
Details	240	65	hsa-miR-589-5p	RBFA	ribosome binding factor A
Details	241	65	hsa-miR-589-5p	AVL9	AVL9 cell migration associated
Details	242	65	hsa-miR-589-5p	NEPRO	nucleolus and neural progenitor protein
Details	243	65	hsa-miR-589-5p	DPY19L4	dpy-19 like 4
Details	244	65	hsa-miR-589-5p	CASP9	caspase 9
Details	245	65	hsa-miR-589-5p	SLC30A6	solute carrier family 30 member 6
Details	246	65	hsa-miR-589-5p	KCNC1	potassium voltage-gated channel subfamily C member 1
Details	247	64	hsa-miR-589-5p	PHC3	polyhomeotic homolog 3
Details	248	64	hsa-miR-589-5p	CAPRIN1	cell cycle associated protein 1
Details	249	64	hsa-miR-589-5p	MLEC	Malectin
Details	250	64	hsa-miR-589-5p	HELZ	helicase with zinc finger
Details	251	64	hsa-miR-589-5p	SYNJ2	synaptojanin 2
Details	252	64	hsa-miR-589-5p	VEZT	vezatin, adherens junctions transmembrane protein
Details	253	64	hsa-miR-589-5p	NUDT16	nudix hydrolase 16
Details	254	64	hsa-miR-589-5p	ZNF697	zinc finger protein 697
Details	255	64	hsa-miR-589-5p	PHF14	PHD finger protein 14
Details	256	64	hsa-miR-589-5p	C4orf3	chromosome 4 open reading frame 3
Details	257	63	hsa-miR-589-5p	RD3	retinal degeneration 3, GUCY2D regulator
Details	258	63	hsa-miR-589-5p	CDC37L1	cell division cycle 37 like 1
Details	259	63	hsa-miR-589-5p	DDHD1	DDHD domain containing 1

Details	260	63	hsa-miR-589-5p	VPS26A	VPS26, retromer complex component A
Details	261	63	hsa-miR-589-5p	CYTH1	cytohesin 1
Details	262	63	hsa-miR-589-5p	ITFG1	integrin alpha FG-GAP repeat containing 1
Details	263	63	hsa-miR-589-5p	TRAK1	trafficking kinesin protein 1
Details	264	63	hsa-miR-589-5p	ANO5	anoctamin 5
Details	265	63	hsa-miR-589-5p	ATF7	activating transcription factor 7
Details	266	63	hsa-miR-589-5p	UBE2W	ubiquitin conjugating enzyme E2 W
Details	267	63	hsa-miR-589-5p	KANK1	KN motif and ankyrin repeat domains 1
Details	268	62	hsa-miR-589-5p	SUPT16H	SPT16 homolog, facilitates chromatin remodeling subunit
Details	269	62	hsa-miR-589-5p	ZNF354B	zinc finger protein 354B
Details	270	62	hsa-miR-589-5p	METTL21A	methyltransferase like 21A
Details	271	62	hsa-miR-589-5p	PHETA2	PH domain containing endocytic trafficking adaptor 2
Details	272	62	hsa-miR-589-5p	SDR42E1	short chain dehydrogenase/reductase family 42E, member 1
Details	273	62	hsa-miR-589-5p	GDAP1L1	ganglioside induced differentiation associated protein 1 like 1
Details	274	62	hsa-miR-589-5p	HNRNPD	heterogeneous nuclear ribonucleoprotein D
Details	275	62	hsa-miR-589-5p	GTSF1	gametocyte specific factor 1
Details	276	62	hsa-miR-589-5p	ZBTB44	zinc finger and BTB domain containing 44
Details	277	62	hsa-miR-589-5p	LONP2	lon peptidase 2, peroxisomal
Details	278	62	hsa-miR-589-5p	ZNF365	zinc finger protein 365
Details	279	62	hsa-miR-589-5p	ACER3	alkaline ceramidase 3
Details	280	62	hsa-miR-589-5p	SLITRK4	SLIT and NTRK like family member 4
Details	281	61	hsa-miR-589-5p	MS4A1	membrane spanning 4-domains A1
Details	282	61	hsa-miR-589-5p	VASN	Vasorin
Details	283	61	hsa-miR-589-5p	DUSP14	dual specificity phosphatase 14
Details	284	61	hsa-miR-589-5p	SIDT1	SID1 transmembrane family member 1
Details	285	61	hsa-miR-589-5p	TPCN2	two pore segment channel 2
Details	286	61	hsa-miR-589-5p	ATP2B4	ATPase plasma membrane Ca2+ transporting 4
Details	287	61	hsa-miR-589-5p	KIF18A	kinesin family member 18A
Details	288	61	hsa-miR-589-5p	PFKFB2	6-phosphofructo-2-kinase/fructose-2,6-biphosphatase 2
Details	289	61	hsa-miR-589-5p	BEST4	bestrophin 4
Details	290	61	hsa-miR-589-5p	TMEM163	transmembrane protein 163
Details	291	61	hsa-miR-589-5p	IVD	isovaleryl-CoA dehydrogenase
Details	292	61	hsa-miR-589-5p	CNOT6	CCR4-NOT transcription complex subunit 6
Details	293	61	hsa-miR-589-5p	MED4	mediator complex subunit 4
Details	294	60	hsa-miR-589-5p	CDKL5	cyclin dependent kinase like 5
Details	295	60	hsa-miR-589-5p	C1GALT1	core 1 synthase, glycoprotein-N-acetylgalactosamine 3-beta-galactosyltransferase 1
Details	296	60	hsa-miR-589-5p	FAM110C	family with sequence similarity 110 member C

Details	297	60	hsa-miR-589-5p	PCM1	pericentriolar material 1
Details	298	60	hsa-miR-589-5p	PCNX4	pecanex 4
Details	299	60	hsa-miR-589-5p	HNRNPR	heterogeneous nuclear ribonucleoprotein R
Details	300	60	hsa-miR-589-5p	FUT3	fucosyltransferase 3 (Lewis blood group)
Details	301	60	hsa-miR-589-5p	HIF1AN	hypoxia inducible factor 1 subunit alpha inhibitor
Details	302	59	hsa-miR-589-5p	TSPAN11	tetraspanin 11
Details	303	59	hsa-miR-589-5p	FAM72B	family with sequence similarity 72 member B
Details	304	59	hsa-miR-589-5p	USP32	ubiquitin specific peptidase 32
Details	305	59	hsa-miR-589-5p	CAMK2D	calcium/calmodulin dependent protein kinase II delta
Details	306	59	hsa-miR-589-5p	TRIM2	tripartite motif containing 2
Details	307	59	hsa-miR-589-5p	FAM72C	family with sequence similarity 72 member C
Details	308	59	hsa-miR-589-5p	FAM72A	family with sequence similarity 72 member A
Details	309	59	hsa-miR-589-5p	SERTAD2	SERTA domain containing 2
Details	310	59	hsa-miR-589-5p	HCAR1	hydroxycarboxylic acid receptor 1
Details	311	59	hsa-miR-589-5p	IRS1	insulin receptor substrate 1
Details	312	59	hsa-miR-589-5p	TAF9B	TATA-box binding protein associated factor 9b
Details	313	59	hsa-miR-589-5p	PIP5K1C	phosphatidylinositol-4-phosphate 5-kinase type 1 gamma
Details	314	59	hsa-miR-589-5p	RP1	RP1, axonemal microtubule associated
Details	315	59	hsa-miR-589-5p	FAM72D	family with sequence similarity 72 member D
Details	316	59	hsa-miR-589-5p	SYNPO2	synaptopodin 2
Details	317	59	hsa-miR-589-5p	AUTS2	AUTS2, activator of transcription and developmental regulator
Details	318	59	hsa-miR-589-5p	MAPK14	mitogen-activated protein kinase 14
Details	319	58	hsa-miR-589-5p	F9	coagulation factor IX
Details	320	58	hsa-miR-589-5p	GALNT10	polypeptide N-acetylgalactosaminyltransferase 10
Details	321	58	hsa-miR-589-5p	MARCH6	membrane associated ring-CH-type finger 6
Details	322	58	hsa-miR-589-5p	PRTG	protogenin
Details	323	58	hsa-miR-589-5p	PLCXD3	phosphatidylinositol specific phospholipase C X domain containing 3
Details	324	58	hsa-miR-589-5p	FBXL18	F-box and leucine rich repeat protein 18
Details	325	58	hsa-miR-589-5p	DGKG	diacylglycerol kinase gamma
Details	326	58	hsa-miR-589-5p	TAPBP	TAP binding protein
Details	327	58	hsa-miR-589-5p	ATP2B2	ATPase plasma membrane Ca2+ transporting 2
Details	328	58	hsa-miR-589-5p	SPOP	speckle type BTB/POZ protein
Details	329	58	hsa-miR-589-5p	TBC1D10B	TBC1 domain family member 10B
Details	330	57	hsa-miR-589-5p	FUK	fucokinase
Details	331	57	hsa-miR-589-5p	PITPNB	phosphatidylinositol transfer protein beta
Details	332	57	hsa-miR-589-5p	CDHR3	cadherin related family member 3
Details	333	57	hsa-miR-589-5p	EYA4	EYA transcriptional coactivator and phosphatase 4

Details	334	57	hsa-miR-589-5p	DCHS1	dachsous cadherin-related 1
Details	335	57	hsa-miR-589-5p	BMPER	BMP binding endothelial regulator
Details	336	57	hsa-miR-589-5p	OTUD7B	OTU deubiquitinase 7B
Details	337	57	hsa-miR-589-5p	GPM6B	glycoprotein M6B
Details	338	57	hsa-miR-589-5p	PRR15	proline rich 15
Details	339	57	hsa-miR-589-5p	CTSE	cathepsin E
Details	340	56	hsa-miR-589-5p	SRCIN1	SRC kinase signaling inhibitor 1
Details	341	56	hsa-miR-589-5p	ZNF324B	zinc finger protein 324B
Details	342	56	hsa-miR-589-5p	CANT1	calcium activated nucleotidase 1
Details	343	56	hsa-miR-589-5p	ZNF506	zinc finger protein 506
Details	344	56	hsa-miR-589-5p	CCNA2	cyclin A2
Details	345	56	hsa-miR-589-5p	HDAC3	histone deacetylase 3
Details	346	56	hsa-miR-589-5p	RNF169	ring finger protein 169
Details	347	56	hsa-miR-589-5p	ALG13	ALG13, UDP-N-acetylglucosaminyltransferase subunit
Details	348	56	hsa-miR-589-5p	STIM2	stromal interaction molecule 2
Details	349	55	hsa-miR-589-5p	SESTD1	SEC14 and spectrin domain containing 1
Details	350	55	hsa-miR-589-5p	MTG2	mitochondrial ribosome associated GTPase 2
Details	351	55	hsa-miR-589-5p	FOSB	FosB proto-oncogene, AP-1 transcription factor subunit
Details	352	55	hsa-miR-589-5p	PRCP	prolylcarboxypeptidase
Details	353	55	hsa-miR-589-5p	FBXO32	F-box protein 32
Details	354	55	hsa-miR-589-5p	RIMS2	regulating synaptic membrane exocytosis 2
Details	355	55	hsa-miR-589-5p	ZBTB45	zinc finger and BTB domain containing 45
Details	356	55	hsa-miR-589-5p	ALX4	ALX homeobox 4
Details	357	55	hsa-miR-589-5p	FBXO45	F-box protein 45
Details	358	55	hsa-miR-589-5p	SHC3	SHC adaptor protein 3
Details	359	55	hsa-miR-589-5p	ZNF208	zinc finger protein 208
Details	360	55	hsa-miR-589-5p	SHC2	SHC adaptor protein 2
Details	361	55	hsa-miR-589-5p	CBX5	chromobox 5
Details	362	55	hsa-miR-589-5p	HECTD4	HECT domain E3 ubiquitin protein ligase 4
Details	363	55	hsa-miR-589-5p	WDR33	WD repeat domain 33
Details	364	54	hsa-miR-589-5p	STK10	serine/threonine kinase 10
Details	365	54	hsa-miR-589-5p	RTN3	reticulon 3
Details	366	54	hsa-miR-589-5p	SUCLG2	succinate-CoA ligase GDP-forming beta subunit
Details	367	54	hsa-miR-589-5p	ARMC10	armadillo repeat containing 10
Details	368	54	hsa-miR-589-5p	LRRK1	leucine rich repeat kinase 1
Details	369	54	hsa-miR-589-5p	NIT2	nitrilase family member 2
Details	370	54	hsa-miR-589-5p	DCAF12	DDB1 and CUL4 associated factor 12
Details	371	54	hsa-miR-589-5p	RBM12B	RNA binding motif protein 12B

Details	372	54	hsa-miR-589-5p	HLA-DOA	major histocompatibility complex, class II, DO alpha
Details	373	54	hsa-miR-589-5p	RAPGEF6	Rap guanine nucleotide exchange factor 6
Details	374	54	hsa-miR-589-5p	SYN1	synapsin I
Details	375	54	hsa-miR-589-5p	TXNL4B	thioredoxin like 4B
Details	376	54	hsa-miR-589-5p	SIAH2	siah E3 ubiquitin protein ligase 2
Details	377	54	hsa-miR-589-5p	LEPROT	leptin receptor overlapping transcript
Details	378	54	hsa-miR-589-5p	AK5	adenylate kinase 5
Details	379	54	hsa-miR-589-5p	FOXQ1	forkhead box Q1
Details	380	54	hsa-miR-589-5p	LPAR5	lysophosphatidic acid receptor 5
Details	381	53	hsa-miR-589-5p	MINDY1	MINDY lysine 48 deubiquitinase 1
Details	382	53	hsa-miR-589-5p	APPL1	adaptor protein, phosphotyrosine interacting with PH domain and leucine zipper 1
Details	383	53	hsa-miR-589-5p	ADARB1	adenosine deaminase, RNA specific B1
Details	384	53	hsa-miR-589-5p	HEG1	heart development protein with EGF like domains 1
Details	385	53	hsa-miR-589-5p	POMZP3	POM121 and ZP3 fusion
Details	386	53	hsa-miR-589-5p	PCDH19	protocadherin 19
Details	387	53	hsa-miR-589-5p	RNF217	ring finger protein 217
Details	388	53	hsa-miR-589-5p	DTD1	D-tyrosyl-tRNA deacylase 1
Details	389	53	hsa-miR-589-5p	ADAR	adenosine deaminase, RNA specific
Details	390	53	hsa-miR-589-5p	SMIM6	small integral membrane protein 6
Details	391	53	hsa-miR-589-5p	ARFGEF2	ADP ribosylation factor guanine nucleotide exchange factor 2
Details	392	53	hsa-miR-589-5p	PNPO	pyridoxamine 5'-phosphate oxidase
Details	393	53	hsa-miR-589-5p	LRRN4CL	LRRN4 C-terminal like
Details	394	53	hsa-miR-589-5p	MTAP	methylthioadenosine phosphorylase
Details	395	53	hsa-miR-589-5p	PLSCR4	phospholipid scramblase 4
Details	396	53	hsa-miR-589-5p	FADD	Fas associated via death domain
Details	397	53	hsa-miR-589-5p	TRIM27	tripartite motif containing 27
Details	398	53	hsa-miR-589-5p	SLF2	SMC5-SMC6 complex localization factor 2
Details	399	53	hsa-miR-589-5p	BCL11A	BCL11A, BAF complex component
Details	400	52	hsa-miR-589-5p	FAM50B	family with sequence similarity 50 member B
Details	401	52	hsa-miR-589-5p	CCK	cholecystokinin
Details	402	52	hsa-miR-589-5p	DIS3	DIS3 homolog, exosome endoribonuclease and 3'-5' exoribonuclease
Details	403	52	hsa-miR-589-5p	LOC110117498-PIK3R3	LOC110117498-PIK3R3 readthrough
Details	404	52	hsa-miR-589-5p	AMPH	amphiphysin
Details	405	52	hsa-miR-589-5p	PIK3R3	phosphoinositide-3-kinase regulatory subunit 3
Details	406	52	hsa-miR-589-5p	C17orf107	chromosome 17 open reading frame 107
Details	407	52	hsa-miR-589-5p	NIPSNAP3A	nipsnap homolog 3A
Details	408	52	hsa-miR-589-5p	EFNB2	ephrin B2
Details	409	52	hsa-miR-589-5p	AKR7A2	aldo-keto reductase family 7 member A2
Details	410	52	hsa-miR-589-5p	HTRA3	HtrA serine peptidase 3

Details	411	52	hsa-miR-589-5p	LIN7A	lin-7 homolog A, crumbs cell polarity complex component
Details	412	52	hsa-miR-589-5p	FGFBP3	fibroblast growth factor binding protein 3
Details	413	52	hsa-miR-589-5p	NIN	ninein
Details	414	52	hsa-miR-589-5p	SLC36A4	solute carrier family 36 member 4
Details	415	52	hsa-miR-589-5p	TMC2	transmembrane channel like 2
Details	416	52	hsa-miR-589-5p	NXN	nucleoredoxin
Details	417	51	hsa-miR-589-5p	EHMT2	euchromatic histone lysine methyltransferase 2
Details	418	51	hsa-miR-589-5p	ANO10	anoctamin 10
Details	419	51	hsa-miR-589-5p	CADPS2	calcium dependent secretion activator 2
Details	420	51	hsa-miR-589-5p	VWC2	von Willebrand factor C domain containing 2
Details	421	51	hsa-miR-589-5p	UPP2	uridine phosphorylase 2
Details	422	51	hsa-miR-589-5p	TRAF3IP2	TRAF3 interacting protein 2
Details	423	51	hsa-miR-589-5p	TNNI1	troponin I1, slow skeletal type
Details	424	51	hsa-miR-589-5p	PAPPA	pappalysin 1
Details	425	51	hsa-miR-589-5p	AKAP1	A-kinase anchoring protein 1
Details	426	51	hsa-miR-589-5p	CUL5	cullin 5
Details	427	51	hsa-miR-589-5p	IKZF3	IKAROS family zinc finger 3
Details	428	51	hsa-miR-589-5p	CYB5R2	cytochrome b5 reductase 2
Details	429	51	hsa-miR-589-5p	RNF213	ring finger protein 213
Details	430	51	hsa-miR-589-5p	MME	membrane metalloendopeptidase
Details	431	51	hsa-miR-589-5p	DCLRE1B	DNA cross-link repair 1B
Details	432	51	hsa-miR-589-5p	C20orf203	chromosome 20 open reading frame 203
Details	433	51	hsa-miR-589-5p	PPP2R3A	protein phosphatase 2 regulatory subunit B''alpha
Details	434	51	hsa-miR-589-5p	TBX3	T-box 3
Details	435	51	hsa-miR-589-5p	PEG3	paternally expressed 3
Details	436	51	hsa-miR-589-5p	FBXL22	F-box and leucine rich repeat protein 22
Details	437	51	hsa-miR-589-5p	FAM234B	family with sequence similarity 234 member B
Details	438	51	hsa-miR-589-5p	MREG	Melanoregulin
Details	439	50	hsa-miR-589-5p	BPGM	bisphosphoglycerate mutase
Details	440	50	hsa-miR-589-5p	PDPR	pyruvate dehydrogenase phosphatase regulatory subunit
Details	441	50	hsa-miR-589-5p	THTPA	thiamine triphosphatase
Details	442	50	hsa-miR-589-5p	SEC14L4	SEC14 like lipid binding 4
Details	443	50	hsa-miR-589-5p	PDHA1	pyruvate dehydrogenase E1 alpha 1 subunit
Details	444	50	hsa-miR-589-5p	NBR1	NBR1, autophagy cargo receptor
Details	445	50	hsa-miR-589-5p	ZDHHC17	zinc finger DHHC-type containing 17
Details	446	50	hsa-miR-589-5p	LZTS3	leucine zipper tumor suppressor family member 3
Details	447	50	hsa-miR-589-5p	DNMT3A	DNA methyltransferase 3 alpha

Details	448	50	hsa-miR-589-5p	HIPK3	homeodomain interacting protein kinase 3
Details	449	50	hsa-miR-589-5p	RDX	Radixin
Details	450	50	hsa-miR-589-5p	SSR3	signal sequence receptor subunit 3
Details	451	50	hsa-miR-589-5p	FAM210A	family with sequence similarity 210 member A

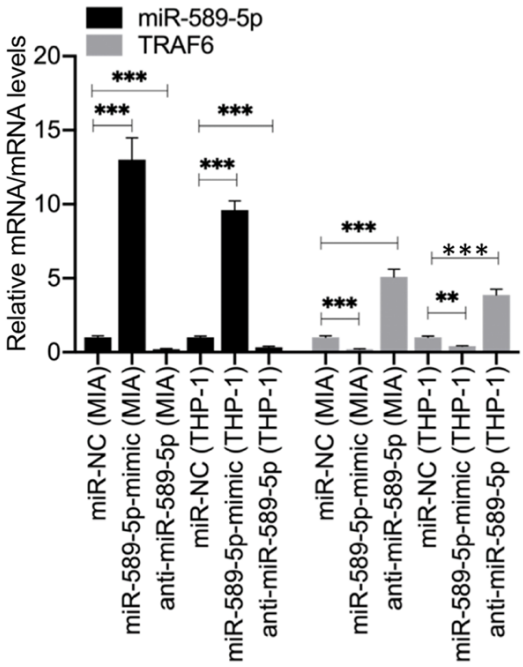

Figure S2. The expression of miR-589-5p and TRAF6 in THP-1 and MIA PaCa-2 cells transfected with miR-589-mimic or anti-miR-589. The THP-1 and MIA PaCa-2 cells were transfected with miR-589-mimic or anti-miR-589. After incubating for 48 h, cells were used for RNA isolation, followed by qRT-PCR analyses to examine the expression levels of miR-589-5p and *TRAF6*. ***P < 0.001.

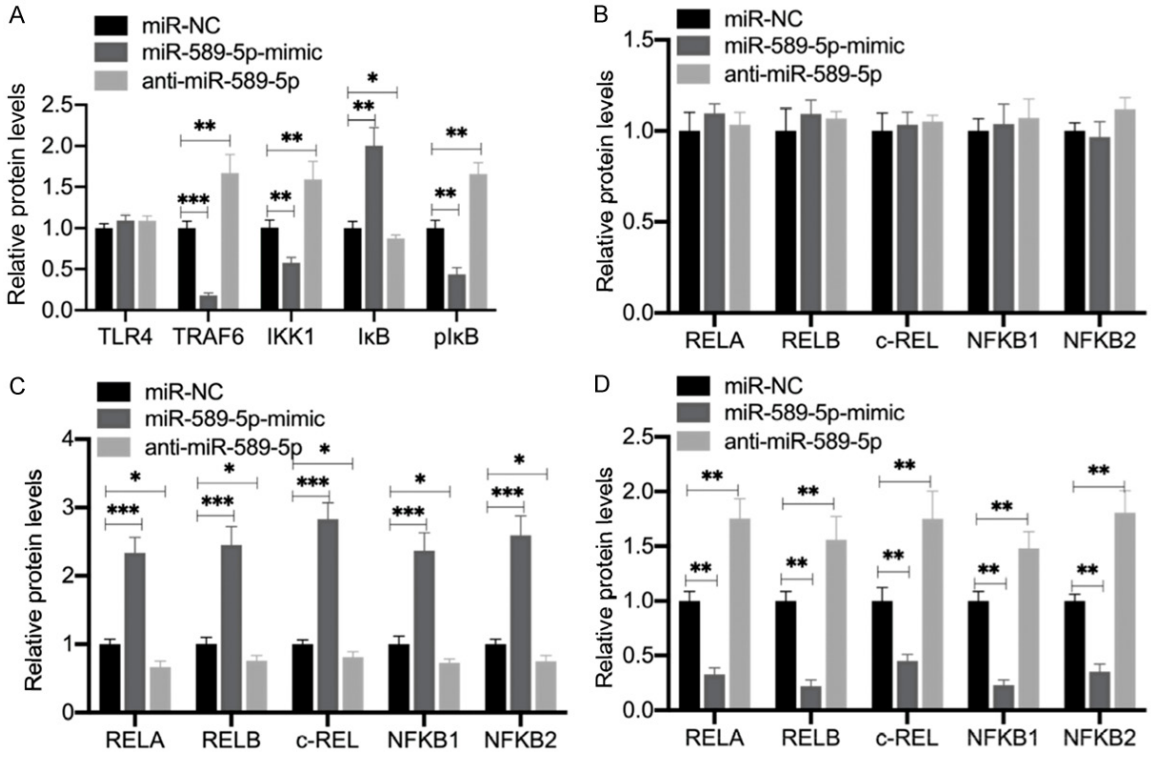

Figure S3. Quantification of the protein levels of members of the TLR4/NF-kB signaling pathway and NF-kB subunits in cells overexpressing or downregulating miR-589-5p. The protein levels in **Figure 5** were quantified using ImageJ software. The signal intensity of individual proteins was normalized to the loading controls. A. The relative protein levels in **Figure 5A**. *P < 0.05, **P < 0.01, and ***P < 0.001. B. The relative protein levels in **Figure 5B**. C. The relative protein levels in **Figure 5C**. *P < 0.05 and ***P < 0.001. D. The relative protein levels in **Figure 5D**. **P < 0.01.

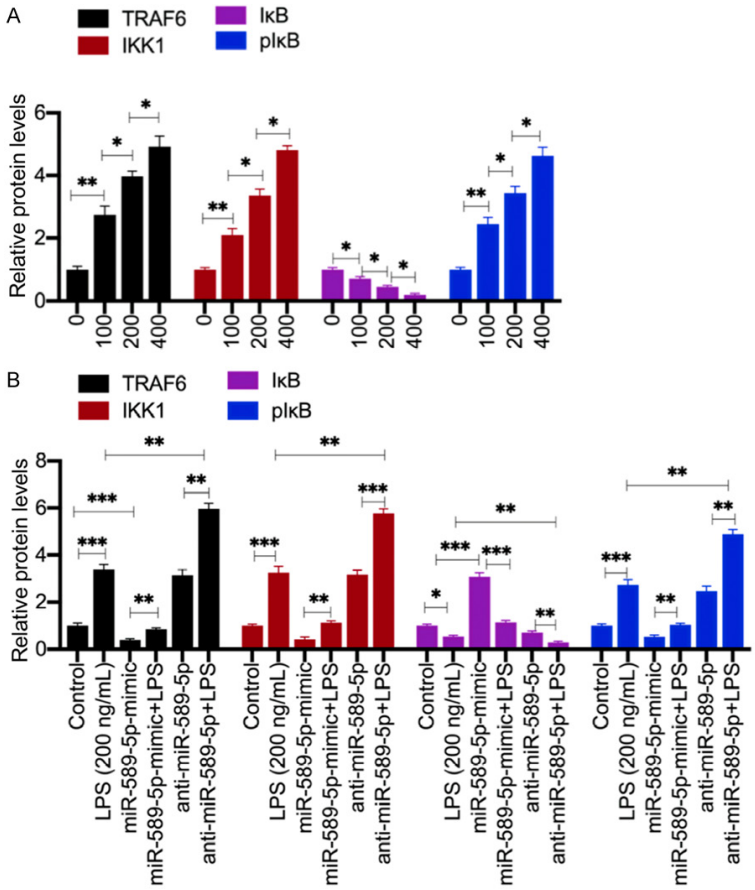

Figure S4. Quantification of the protein levels of members of the TLR4/NF-kB signaling pathway in cells treated with LPS or LPS+anti-miR-589-5p. The protein levels in **Figure 6** were quantified using ImageJ software. The signal intensity of individual proteins was normalized to the loading controls. A. The relative protein levels in **Figure 6B**. **P* < 0.05 and ** *P* < 0.01. B. The relative protein levels in **Figure 6D**. **P* < 0.05, ** *P* < 0.01 and *** *P* < 0.001.

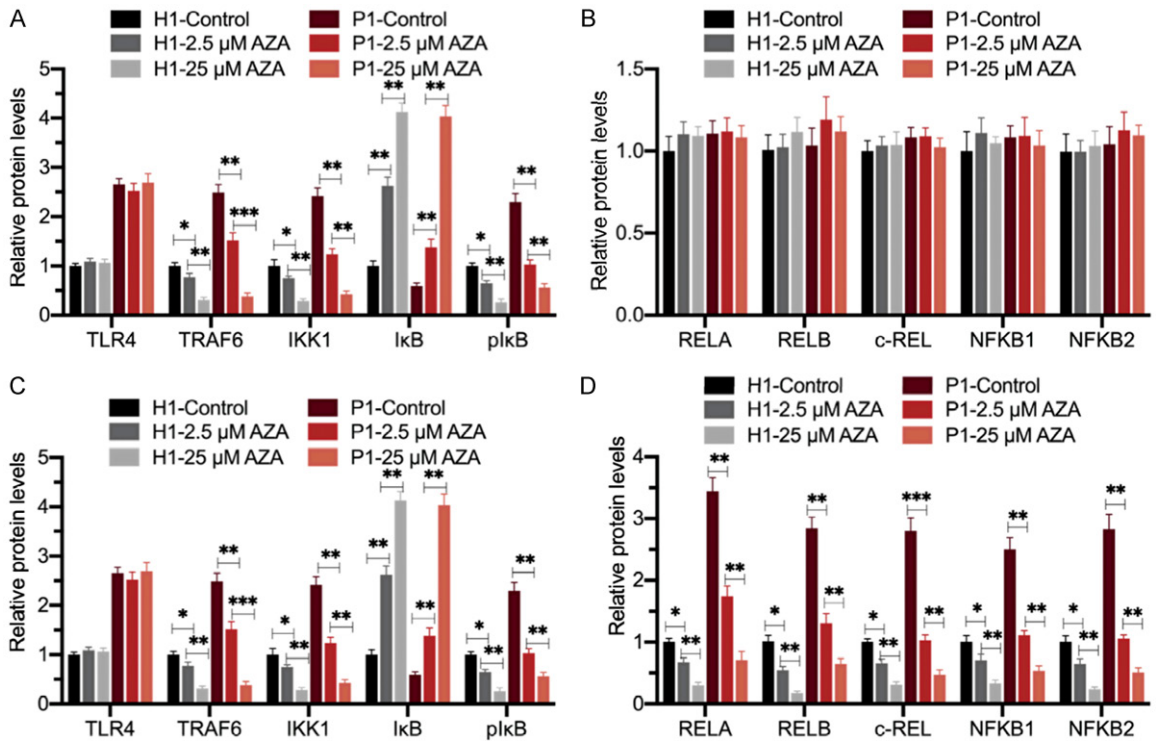

Figure S5. Quantification of the protein levels of members of the TLR4/NF-kB signaling pathway and NF-kB subunits in cells treated with AZA. The protein levels in **Figure 8** were quantified using ImageJ software. The signal intensity of individual proteins was normalized to the loading controls. A. The relative protein levels in **Figure 8A**. **P* < 0.05 and ***P* < 0.01. B. The relative protein levels in **Figure 8B**. C. The relative protein levels in **Figure 8C**. **P* < 0.05, ***P* < 0.01 and ****P* < 0.001. D. The relative protein levels in **Figure 8D**. **P* < 0.05 and ***P* < 0.01.